Review article

Yasutomo Ota*, Kenta Takata, Tomoki Ozawa, Alberto Amo, Zhetao Jia, Boubacar Kante, Masaya Notomi, Yasuhiko Arakawa and Satoshi Iwamoto*

Active topological photonics

https://doi.org/10.1515/nanoph-2019-0376
Received September 20, 2019; revised November 14, 2019; accepted December 4, 2019

Abstract: Topological photonics emerged as a novel route to engineer the flow of light. Topologically protected photonic edge modes, which are supported at the perimeters of topologically nontrivial insulating bulk structures, are of particular interest as they may enable low-loss optical waveguides immune to structural disorder. Very recently, there has been a sharp rise of interest in introducing gain materials into such topological photonic structures, primarily aiming at revolutionizing semiconductor lasers with the aid of physical mechanisms existing in topological physics. Examples of remarkable realizations are topological lasers with unidirectional light output under time-reversal symmetry breaking and topologically protected polariton and micro/nanocavity lasers. Moreover, the introduction of gain and loss provides a fascinating playground to explore novel topological phases, which are in close relevance to non-Hermitian and parity-time symmetric quantum physics and are, in general, difficult to access using fermionic condensed matter systems. Here, we review the cutting-edge research on active topological photonics, in which optical gain plays a pivotal role. We discuss recent realizations of topological lasers of various kinds, together with the underlying physics explaining the emergence of topological edge modes. In such demonstrations, the optical modes of the topological lasers are determined by the dielectric structures and support lasing oscillation with the help of optical gain. We also address recent research on topological photonic systems in which gain and loss, themselves, essentially influence topological properties of the bulk systems. We believe that active topological photonics provides powerful means to advance micro/nanophotonics systems for diverse applications and topological physics, itself, as well.

Keywords: topological physics; nanophotonics; semiconductor lasers; microcavity lasers; photonic crystals; non-Hermitian photonics.

***Corresponding authors: Yasutomo Ota,** Institute for Nano Quantum Information Electronics, The University of Tokyo, 4-6-1 Komaba, Meguro-ku, Tokyo, 153-8505, Japan, e-mail: ota@iis.u-tokyo.ac.jp. https://orcid.org/0000-0002-0869-8998; and
Satoshi Iwamoto, Institute for Nano Quantum Information Electronics, The University of Tokyo, 4-6-1 Komaba, Meguro-ku, Tokyo, 153-8505, Japan; Institute of Industrial Science, The University of Tokyo, 4-6-1 Komaba, Meguro-ku, Tokyo, 153-8505, Japan; and Research Center for Advanced Science and Technology, The University of Tokyo, 4-6-1 Komaba, Meguro-ku, Tokyo, 153-8505, Japan, e-mail: iwamoto@iis.u-tokyo.ac.jp
Kenta Takata: NTT Basic Research Laboratories, NTT Corporation, 3-1 Morinosato-Wakamiya, Atsugi 243-0198, Kanagawa, Japan
Tomoki Ozawa: Interdisciplinary Theoretical and Mathematical Sciences Program Mathematical Sciences Program (iTHEMS), RIKEN, Wako, Saitama 351-0198, Japan
Alberto Amo: Université de Lille, CNRS, UMR 8523 – PhLAM – Physique des Lasers, Atomes et Molécules, Lille, France
Zhetao Jia and Boubacar Kante: Electrical Engineering and Computer Sciences, University of California Berkeley, Berkeley, CA, USA
Masaya Notomi: NTT Basic Research Laboratories, NTT Corporation, 3-1 Morinosato-Wakamiya, Atsugi 243-0198, Kanagawa, Japan; and Department of Physics, Tokyo Institute of Technology, H-55, Ookayama 2-12-1, Meguro 152-8550, Tokyo, Japan
Yasuhiko Arakawa: Institute for Nano Quantum Information Electronics, The University of Tokyo, 4-6-1 Komaba, Meguro-ku, Tokyo, 153-8505, Japan

1 Introduction

The search for novel ways to manipulate light with optical structures is a central focus of research in photonics. Topological photonics was a key framework for such studies for recent years and keeps growing as a resource of novel concepts for advancing photonic devices, such as waveguides, beam splitters, isolators, and resonators. Two-dimensional (2D) photonic systems analogous to quantum Hall [1–4], quantum spin Hall [5–12], and quantum valley Hall [13–15] systems were proposed and experimentally demonstrated in microwave and/or optical regime. Topological 1D edge states supported at the exterior of the 2D bulk systems may enable topologically protected light transport immune to sharp waveguide bends and structural imperfections as well as unidirectional light transport inhibiting back reflection. Such robust properties, together with emerging novel functionalities, are highly attractive for building

compact, low-loss, and functional photonic integrated circuitry. More recently, there are attempts to revolutionize semiconductor lasers with topological photonics. Topological protection of optical modes could be useful for improving laser performances and may lead to lasers with, e.g. robust single-mode operation. The marriage between optical gain and topological photonic structures is also of interest in exploring novel topological physics. In this review, we overview active topological photonics that primarily explores topological photonic devices incorporating optical gain. Generally, lasers, which make use of the topological nature of the photonic band structure, can be called topological lasers. For most cases discussed in this review, topological lasers have lasing modes from topological edge states. We focus on the introduction of various types of topological lasers reported to date and of topological phenomena that are activated by optical gain. For reviews of topological photonics, itself, and its relevance to topological condensed matter physics, the readers can refer to Refs. [16–24].

Figure 1 displays a summary of different types of topological lasers. A variety of platforms were utilized to demonstrate lasing in topological photonic structures. For supporting 0D edge states, which function as stationary cavity modes, 1D topological chains of optical resonators are frequently employed. Each site cavity can be composed of a micropillar [26] (Figure 1A) or a microring resonator [25, 27] (Figure 1B and C). Replacing the site cavities with a nanoscale cavity enables the formation of topological nanocavity modes [28] (Figure 1D). Another way to realize a topological nanocavity is to utilize 1D topological photonic crystal nanobeams [29] (Figure 1E). The interface of the two topologically distinct nanobeams supports a tightly localized interface state. Increasing the dimensionality, 1D edge modes in 2D bulk systems can be implemented using coupled ring resonators and photonic crystals. The first report on topological lasing in a 2D structure employed a magneto-optical 2D photonic crystal that breaks time-reversal symmetry (TRS), giving rise to a 1D chiral edge mode and resulting unidirectional lasing [30] (Figure 1F). Lasing from helical edge states were also examined with 2D arrays of microring resonators [31] (Figure 1G); such systems can be interpreted as pseudo quantum spin Hall systems and can leverage topological protection for the propagating optical modes even without TRS breaking. Micropillar cavities are also

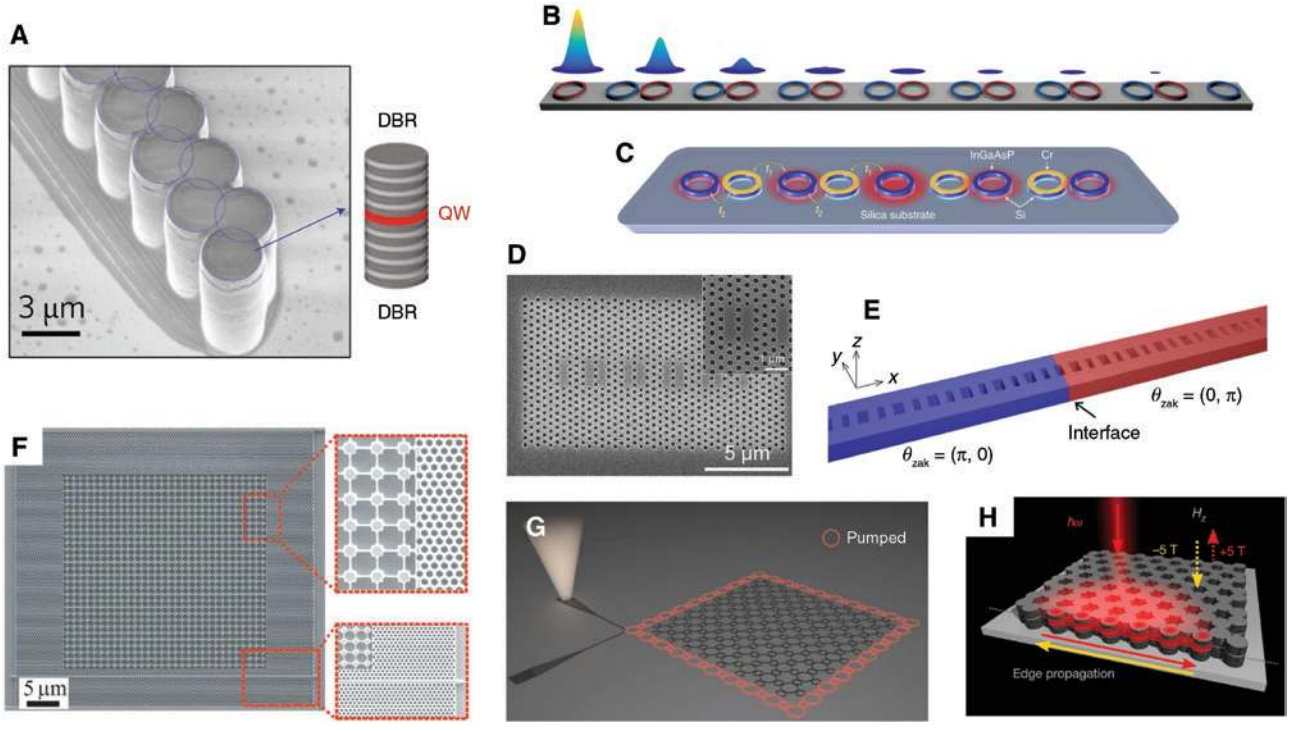

Figure 1: Topological laser structures.
1D arrays of (A) micropillar cavities, (B, C) microring cavities, and (D) photonic crystal nanocavities. (E) 1D photonic crystal nanobeam with a topological disorder. (F) 2D photonic crystal forming a microring resonator with a 1D edge channel. 2D arrays of (G) microring resonators and (H) micropillars. Drawing (B) is provided courtesy of M. Parto et al., the authors of Ref. [25]. Adapted from Ref. [26] for (A), Ref. [27] for (C), Ref. [28] for (D), Ref. [29] for (E), Ref. [30] for (F), Ref. [31] for (G), and Ref [32] for (H).

suitable for forming 2D arrays of coupled optical resonators [32] (Figure 1H).

In the following, we discuss topological lasers with different spatial dimensions and time-space symmetry. We also address novel topological phases emerging under the presence of gain and loss. In Section 2, we discuss topological microcavity and microring lasers based on 0D edge states accompanied with 1D topological bulk systems. Section 3 is devoted to topological nanocavity lasers, with particular focus on the system supporting 0D edge states formed between topological photonic crystal nanobeams. In Section 4, we discuss topological microring lasers based on 1D edge channels in 2D topological bulk systems with broken TRS. Section 5 reviews topological lasers implementing pseudo quantum spin Hall systems that preserve TRS. Section 6 introduces non-Hermitian topological phases enabled by gain and loss, and outlines emergent symmetry classes, together with redefined photonic bandgaps in non-Hermitian physics. Section 7 provides a summary together with a brief outlook of the field.

In this review, we focus on topology in momentum space; we do not cover active systems involving topological charge in real space [33–35]. We note that active topological photonics also led to a variety of unique photonic systems, such as topological photonic waveguides interacting with quantum emitters [11, 36] and those generating quantum light via nonlinear optical processes [37, 38], and topological photonic structures subject to active temporal phase/intensity modulation [39–41] (or Floquet engineering); readers can refer to original or other review papers for these topics.

2 One-dimensional topological microcavity and microring lasers

The first geometry in which lasing in topological edge states was demonstrated is a 1D lattice of coupled photonic resonators implementing the Su-Schrieffer-Heeger (SSH) Hamiltonian [25–27]. This tight-binding model was initially introduced to describe the electronic transport in the polyacetylene molecules, and it provides one of the simplest lattice models with topological properties. The SSH lattice is schematically displayed in Figure 2A. Each unit cell consists of two sites with the same onsite energy (we take it as zero) forming a 1D chain in which the intracell hopping t is different from the intercell hopping t'. In momentum space, in the basis of the A and B sites of each unit cell of size a, the Hamiltonian can be written as [42]:

$$H(k)=\begin{pmatrix} 0 & t+t'e^{ika} \\ t+t'e^{-ika} & 0 \end{pmatrix}$$

The spectrum presents two symmetric bands separated by a gap of width $2|t-t'|$ (Figure 2B). The eigenfunctions of the upper (+) and lower (–) bands are [43]: $|\pm\rangle = 2^{-1/2}(e^{-i\phi(k)}, \pm 1)^{\dagger}$, with $\cot\,\phi(k) = t/(t'\,\sin\,ka) + \cot\,ka$. The phase and symmetry of the eigenfunctions depends on the relative value of t to t'. The topological properties of the Hamiltonian are revealed via the winding $\mathcal{W}$ of the phase $\phi(k)$ across the Brillouin zone [43]:

$$\mathcal{W}=\frac{1}{2}\int_0^{\frac{2\pi}{a}}\frac{\partial\phi(k)}{\partial k}dk.$$

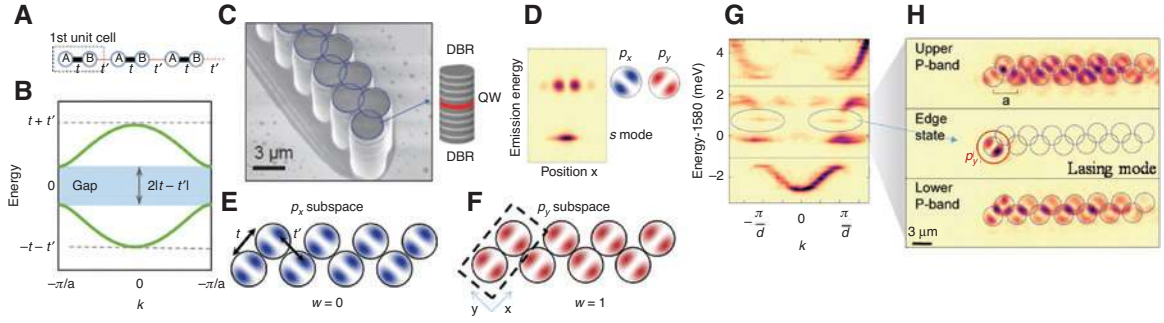

Figure 2: 1D topological microcavity polariton laser.
(A) Scheme of the SSH lattice, defined by two sites per unit cell (A and B) and alternating hopping t and t'. (B) Spectrum of the eigenstates of the SSH Hamiltonian when $t \neq t'$. (C) Realization of the SSH Hamiltonian for p modes in a zigzag chain of coupled micropillars. (D) Emitted photoluminescence from a single micropillar, showing gapped s and p modes. (E, F) Schematic representation of the p_x and p_y subspaces of the zigzag chain. Each subspace implements an SSH chain with different winding. (G) Photoluminescence intensity from the zigzag chain in momentum space. It shows different bands. The middle ones correspond to the p orbitals. Emission from the topological edge state is encircled by blue ellipses. (H) Measured real-space emission at the energy of the lower and upper p bands, and at the energy of the edge state. The edge state has a p_y geometry: this is the sub-space that contains a topological edge state. (C–H) Adapted from Ref. [26].

The winding $\mathcal{W}$ can have two possible values depending on the dimerization: 0 when $t > t'$, and +1 when $t < t'$. These two windings correspond to the two different topological phases of the system. In an infinite lattice, the distinction between the two cases is not relevant as it depends simply on the choice of unit cell, which defines t and t'. However, in a semi-infinite chain, the unit cell is univocally defined by the termination, setting the winding of the chain. When $\mathcal{W} = 0$, the lattice is topologically trivial, and no edge states are expected, but when $\mathcal{W} = +1$, the lattice is topologically non trivial, and a topological state localized at the edge with energy in the middle of the gap ($E = 0$ in our notation) is expected. Similarly, a localized interface state at $E = 0$ appears when joining two semi-infinite SSH chains with different windings [42].

The topological properties of the SSH Hamiltonian are, therefore, very convenient to design structures with isolated states in the middle of the gap. In addition, these states have remarkable robustness to certain types of disorder. The topological properties of the SSH Hamiltonian are intimately related to the chiral symmetry of the Hamiltonian described above, manifested in the fact that the Hamiltonian is purely off-diagonal. The main consequence of the chiral symmetry is that the spectrum is mirror symmetric with respect to $E = 0$: each eigenstate with energy E has a partner eigenstate at energy $-E$. The topological edge or interface state at $E = 0$ is necessarily its own partner, and therefore, its energy is insensitive to any modification of the Hamiltonian that preserves chiral symmetry. In particular, disorder in the hoppings t and t' preserves this symmetry and does not affect the energy of the topological states as long as the gap between the two bands is well defined. On the contrary, the energy of the edge mode is not protected against perturbations that break chiral symmetry. For instance, disorder in the onsite energies will affect the energy of the edge mode.

In optics, the SSH Hamiltonian was implemented making use of lattices of waveguides in fused silica [37, 44, 45], microwave resonators [46], and plasmonic [47] and dielectric nanostructures [48]. However, these systems are passive and cannot be used to implement lasing in edge modes. A successful strategy to circumvent this issue was to use lattices of photonic resonators made of inorganic semiconductors, in which a quantum well layer provides a gain medium. The first system showing lasing in a topologically protected edge state was a 1D lattice of coupled polariton micropillars implementing the SSH Hamiltonian [26]. In this platform, each individual micropillar possesses a series of confined photonic modes with s, p, d, … symmetries (Figure 2D). In Ref. [26], the SSH Hamiltonian is implemented for the p_x and p_y modes, whose spatial shape is strongly asymmetric. To do so, the chain of coupled micropillars was designed in a zigzag geometry (Figure 2C): due to the non-cylindrical shape of the p_x modes, the alternating connecting angles between the micropillars results in mode overlap with alternating strong t and weak t' couplings of photons between adjacent sites (Figure 2E). The opposite arrangement of couplings ($t < t'$) is simultaneously realized for the other set of orbitals (p_y, Figure 2F). Both orbital sub-spaces present the same gap, but for the chain termination shown in Figure 2C, only the p_y subspace has a weak link at the edge and presents a topological edge state (the p_x subspace has a strong link at the edge).

In order to observe lasing from the topological edge mode, St-Jean and co-workers [26] designed a microcavity with a quantum well energy such that the polariton gain was optimized for the energy of the p modes of the lattice. To favor gain in the topological mode vs. the bulk modes, they optically pumped the chain with a spot located close to the edge.

In Refs. [25] and [27], the strategy was to employ the longitudinal photonic modes of evanescently coupled ring resonators made of InGaAsP, a material with optical gain at telecom wavelengths. The alternating couplings t and t' were engineered via the staggered separation between adjacent rings. In the work of Parto et al. [25], shown in Figure 3A–C, the topological state is located at the edge of the chain, where a weak coupling was engineered. The rings were weakly coupled to guided gratings to measure the light intensity in the rings. In the work of Zhao et al. [27], shown in Figure 3D and E, the topological mode is located at the interface between two segments of the lattice with opposite strong/weak coupling dimerizations. In both works, to trigger lasing in the topological mode, the two groups relied on the specific shape of the topological eigenmode: due to the chiral symmetry of the SSH Hamiltonian, the eigenfunction of the topological mode at $E = 0$ is nonzero only in one of the A/B sublattices. In particular, it is nonzero in the sublattice corresponding to the site located at the edge of the lattice [25] or at the interface site [27]. This characteristic is exclusive to that mode; all the bulk modes have components in both sublattices. Therefore, if the gain and losses of each sublattice are engineered to favor gain in the sublattice of the topological mode, lasing in this mode can be observed [49]. In Ref. [25], the authors designed an optical pumping profile such that only the sublattice of the topological mode was pumped, favoring gain in that mode. In Ref. [27], pumping was homogeneously distributed, but losses were enhanced in the sublattice not containing the topological mode. This strategy was already used to enhance the emission for the topological mode in a lattice of microwave resonators with parity-time symmetry [46].

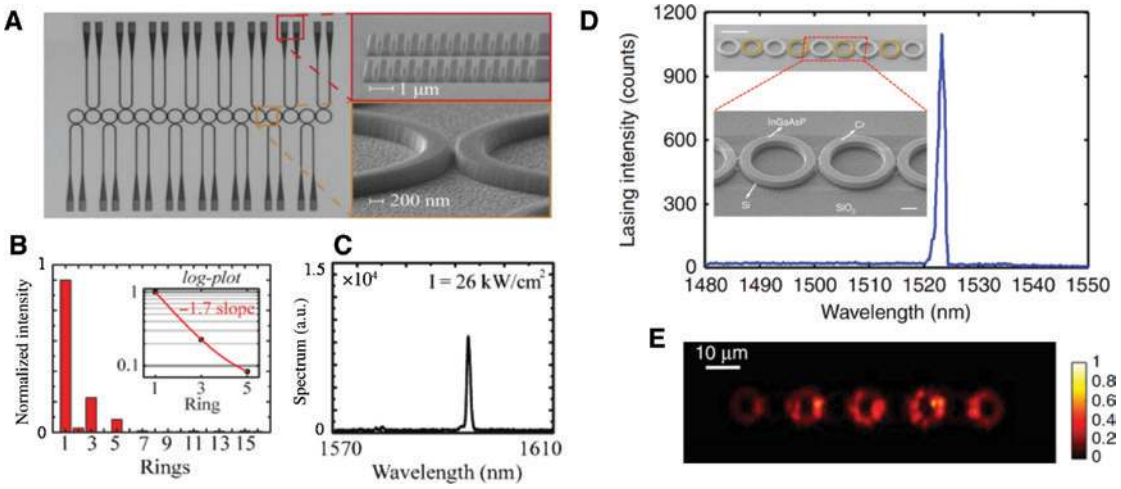

Figure 3: 1D topological microring cavity lasers.
(A) Scanning electron microscope image of the lattice of ring resonators with staggered coupling engineered by Parto et al. [25]. (B) Measured intensity of the lasing mode showing the characteristic sublattice asymmetry of the topological edge state. (C) Spectrum of the topological lasing mode. (D) Measured lasing emission from the interface state engineered by Zhao et al. [27]. The inset shows scanning electron microscope images of the coupled ring resonators fabricated on a SiO_2 substrate. (E) Measured spatial shape of the laser emission centered around a topological interface state. (A–C) Adapted from Ref. [25]. (D, E) Adapted from Ref. [27].

One of the most interesting features explored in the abovementioned works is the resilience of the topological lasing mode to disorder. The chiral symmetry of the lattice Hamiltonian makes the topological mode insensitive to perturbations in the hoppings t and t'. Perturbations in the onsite energies do affect the energy of the topological mode, which can then move up or down. However, as long as those perturbations are smaller than the bandgap, the topological mode is well isolated in the gap, and lasing is preserved. This feature was experimentally demonstrated both in St-Jean et al. [26] and in Zhao et al. [27] by modifying in a controlled way the onsite energy of sites in which the topological state has a significant weight. Compared to Tamm defect modes, which emerge at the band edges when a local perturbation is added at the edge of a chain, the topological modes in a SSH lattice have the advantage of appearing directly in the middle of the gap, well separated from the bands, thus, presenting a much stronger resilience to perturbations of the onsite energy. It has also been studied theoretically that topological lasing in the SSH lattice is stable even in the presence of nonlinearity (saturation) in the gain strength [50].

3 Topological nanocavity lasers

In the previous section, we discussed topological microcavities based on 0D edge states that emerged at the perimeter of 1D bulk systems and their application to topological lasers. From the view point of future applications of topological photonics, in particular, for densely integrated nanophotonic circuits, it is imperative to consider ways to downscale such microcavities to the nanoscale for minimizing their footprints. Smaller cavities also facilitate strong light matter interactions, which improve laser performances such as spontaneous emission coupling factor, leading to low-threshold, low-power-consumption, and high-speed operation. In this section, we review designs to downscale topological cavities to the nanoscale and topological lasers based on them.

A straightforward design to realize a topological nanocavity is to construct a 1D bulk system using nanoscale site resonators. With this strategy, a downsized version of the 1D SSH model discussed in the previous section can be developed. C. Han et al. [28] built an array of defect-based photonic crystal nanocavities that behave as a photonic analog of the SSH model, as shown in Figure 1D. The cavities are formed in an InP-based slab embedding InGaAs quantum wells, which support lasing at 0D topological edge states. The edge states were designed to tightly confine light in a resonator site and, hence, behaved similarly to an isolated defect nanocavity. This design of topological nanocavity results in a high Q factor over 10,000 with a small mode volume comparable to conventional high Q photonic crystal nanocavities, resulting in lasing with a high spontaneous emission coupling factor of ~0.1. In the same scenario, topological plasmonic nanocavities formed at the exterior of plasmonic resonator arrays can be constructed [51], though they have not been examined as laser devices.

Topological nanocavities can also be formed at the interfaces of topologically nontrivial 1D photonic crystals, as schematically shown in Figure 1E. Leveraging the photonic crystal nanobeam geometry, tightly localized nanoscale edge modes with high Q factors over 10,000 were demonstrated [29]. Lasing from this topological nanocavity will be reviewed later in this section. Such structures do not have the chiral symmetry, which was essential in the topology of SSH model. Instead, the photonic crystals hold inversion symmetry and are characterized with quantized Zak phases. A Zak phase, θ_{Zak}, for an optical band of a 1D photonic crystal is defined as follows:

$$\theta_{Zak} = \int_{BZ} i\langle\psi_k|\nabla_k|\psi_k\rangle dk,$$

where $|\psi_k\rangle$ is the Bloch function, θ_{Zak} is the integral of the Berry connection over the Brillouin zone and is equivalent to a Berry phase defined in the momentum space. A nontrivial Zak phase suggests evolution of parity of $|\psi_k\rangle$ in the momentum space. We note that one of the earliest theoretical discussion of lasing in topological edge states was reported in such a continuum photonic crystal structure, where topological edge states of 1D Aubry-André-Harper model was shown to operate as a laser [52].

Photonic crystal waveguides are another 1D platform to implement 0D topological nanocavities. The insertion of air holes with a period different from that of the host photonic crystal into the waveguide is known to result in a system emulating the Aubry-Andre-Harper model [53–55]. In this case, the model mimics a quantum Hall system defined in a pseudo 2D momentum space, where insertion position of the additional air holes takes the role of the momentum in an artificial dimension. Topological edge modes emerge in the virtual space as 1D edge states, which behave as nanocavity modes in the real space with high Q factors over a million.

One of the other possible ideas is corner states in higher-order topological insulators [56, 57], which are under intensive development also in topological photonics [58–65]. Nanocavities based on topological corner states were already demonstrated using 2D topological photonic crystals characterized with nontrivial 2D Zak phases [65]. They can function as nanocavities embedded in 2D systems, offering a natural platform for developing integrated photonic circuits. Meanwhile, one may consider the introduction of defect-based nanocavities into 2D topological photonic crystals by, for example, filling some airholes with dielectric [66] or introducing topological disorder [67]. These types of cavities were far less investigated in the context of topological photonics, despite their possibilities to function as high-performance nanocavities in topological nanophotonic systems.

For the rest of this section, we discuss a laser based on a topological nanocavity formed in a 1D topological photonic crystal [29], as schematically depicted in Figure 1E. The system under consideration is detailed in Figure 4A. The width and thickness of the nanobeam are

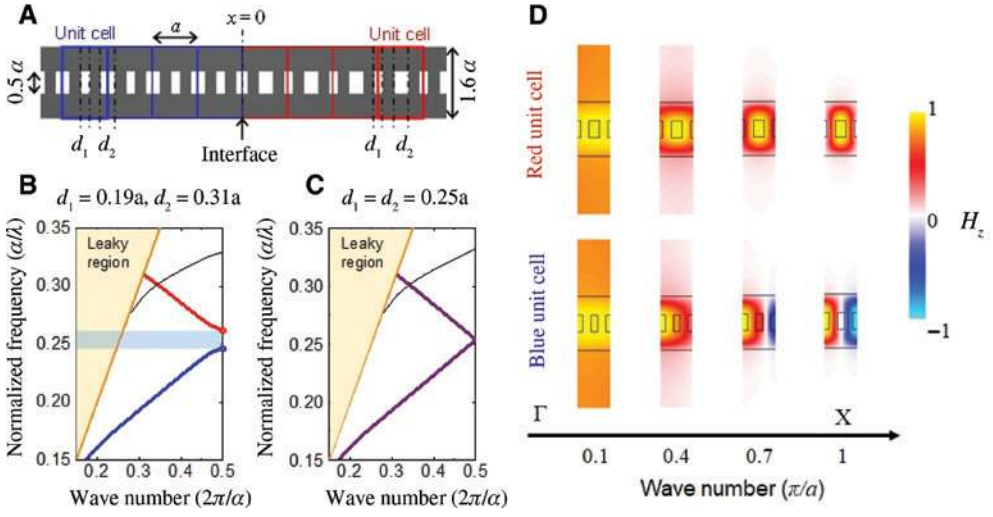

Figure 4: 1D topological photonic crystal nanobeam.
(A) Details of the design of the topological nanocavity based on photonic crystal nanobeams, the schematic of which is depicted in Figure 1E. The interface is formed between a topological photonic crystal based on the blue unit cell and a trivial photonic crystal with the red unit cell. (B) Computed optical bands for the photonic crystal constituted of the blue unit cell with $d_1 = 0.19a$ and $d_2 = 0.31a$. (C) The same in (B) but with $d_1 = d_2 = 0.25a$. (D) Evolution of wavefunctions across the momentum space, calculated for the trivial and topological photonic crystals. (A–C) Reproduced from Ref. [29].

chosen such that it supports only a single transverse-electric-like optical mode with a small mode cross-section. Digging square airholes in the nanobeam results in 1D photonic bandgaps, the topology of which are characterized with the Zak phase [68]. The unit cell contains two air holes located to the positions preserving inversion symmetry, which results in the quantization of the Zak phase to either 0 or π, equivalent to the quantization of the winding number $\mathcal{W}$ defined in the previous section. The relationship between the sizes of the two air holes (d_1, d_2) determines the value of the Zak phase of the optical band.

Figure 4B shows the calculated optical bands for the blue unit cell of the photonic crystal nanobeam with a period of a and air hole sizes of $d_1 = 0.19a$ and $d_2 = 0.31a$ by the 2D plane wave expansion method. A wide bandgap is found between the first and second lowest energy bands. The same band structure is reproduced for the red unit cell, which possesses d_2 air hole at the unit cell center. One of these unit cells coincides with the other after shifting the unit cell center by a half period. This shift causes a change in the Zak phase between 0 to π, hence, corresponding to a change in the band topology between trivial and topological. The gapped topologically distinct phases are connected via the point $d_1 = d_2 = 0.25a$, where the gap closes, and a Dirac point is formed, as shown in Figure 4C. The nontrivial optical band here means the presence of a change in parity of the wavefunction within the band. Figure 4D shows evolutions of wavefunctions for the lowest energy bands of the blue and red photonic crystals. For both cases, the wavefunctions near the zero frequency or around Γ point behave as featureless *s*-wave. For the trivial red photonic crystal, the *s*-wave nature is preserved throughout the band. Meanwhile, for the topological case, transformation of the wave nature can be seen, and an anti-symmetric wavefunction is found at X point.

At the interface between the two photonic crystals with different quantized Zak phases, a single in-gap interface state is deterministically formed. This property is advantageous for photonic applications where the control of the number of modes is imperative. Let us note that contrary to the SSH lattices of photonic resonators discussed in Section 2, the bulk photonic crystals considered here do not hold chiral symmetry. Therefore, the energy of the in-gap state is not pinned to the zero energy [42], and the presence of the mode is guaranteed only when inversion symmetry is preserved. From a device point of view, the robustness of the topological in-gap mode to disorders in this type of photonic crystal remained elusive, and more works are necessary to clarify it. It is noteworthy that the emergence of the topological modes is confirmed even when the period of 1D photonic crystal becomes only a few [69]. There are several physical interpretations for the emergence of the edge mode, such as those based on the presence of edge polarization associated with nontrivial Zak phase [57, 70] and on a soliton formation process via the Jackiw-Rebbi mechanism [42, 67, 71]. According to M. Xiao et al., the current system can be viewed as a Fabry-Pérot resonator with zero cavity length [68]. The photonic crystals function as mirrors with different reflection phases, which are related with the Zak phases. A topological edge mode satisfies the resonance condition, which requires the sum of reflection phases by the two mirrors to be integer multiples of 2π. This condition coincides with the case that the Zak phases of the two photonic crystals differ by π. Indeed, the current structure fulfills this condition and supports one and only one in-gap mode. Figure 5A shows a field distribution of the

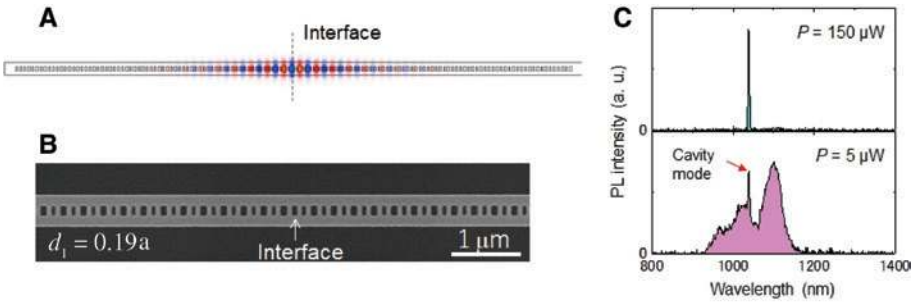

Figure 5: Lasing from a topological nanocavity laser.
(A) Calculated electric field distribution for the topological nanocavity designed with $d_1 = 0.19a$ and $d_2 = 0.31a$. The cavity field is well localized in the vicinity of the interface. (B) Scanning electron microscope image of the fabricated structure. The position of the interface is indicated by an arrow. (C) Emission spectra measured under optical pumping. Bottom: a spectrum taken with a low pump power. Top: a lasing spectrum measured with a high pump power. Clear single-mode lasing can be confirmed by the single cavity peak dominating the spectrum. Reproduced from Ref. [29].

topological interface mode for the design with $d_1 = 0.19a$ and $d_2 = 0.31a$, computed with the 3D finite difference time domain method. The numerically evaluated cavity Q factor is ~60,000, and the mode volume is $0.67(\lambda/n)^3$, where λ is the resonant wavelength, and n is the refractive index of the host material (assuming GaAs). These values are comparable with conventional photonic crystal designs.

Experimentally, the designed topological photonic crystal nanocavity with a period of $a = 270$ nm was formed in a GaAs slab by standard electron beam lithography and dry etching. A scanning electron micrograph of a fabricated sample is shown in Figure 5B. The structure embedded InAs quantum dot as gain medium. The sample was optically characterized under quasi-continuous optical pumping at a cryogenic temperature. The bottom panel of Figure 5C shows a spectrum measured under a low pump power of 5 μW, exhibiting a sharp peak that originated from the topological interface mode, together with broad quantum dot emission background. When increasing the pump power to 150 μW, the device underwent single-mode lasing, the spectrum of which is shown in the upper panel of Figure 5C. A prominent cavity emission peak is observed, while the background emission was strongly suppressed. From a measured light output curve, a high spontaneous emission coupling factor of 0.03 was measured, which indicates enhanced light matter interactions in the device as a result of high experimental Q factor of 9600 and the small mode volume.

4 2D topological laser with TRS breaking

The possibility of opening a topological bandgap in the photonic system by breaking time-reversal symmetry was first proposed in Ref. [1] in analogy to the quantum Hall effect (QHE). The real-structure simulation was reported in Refs. [1] and [72] and implemented at microwave frequency [3], where the photonic crystal structure is made of ferrite rods. In this pioneering work, unidirectional transmission at a frequency within the topological bandgap is demonstrated. Such chiral edge mode is robust in a sense that backscattering is prohibited in the presence of local disorder due to time-reversal symmetry breaking of the system. The unprecedented properties of the topological edge mode bring the interest of making it as a light source, especially a laser [30, 31, 73]. In general, defects and disorders in the laser cavity lead to scattering loss, which degrades the performance of laser by reducing the quality factor and lowering the output efficiency. The chiral edge mode is immune to such backscattering. Besides, the topological edge mode profile depends on the shape of the topological interface, which can be designed to control the radiation pattern of the lasing mode. The lasing process, including the gain competition between the chiral edge mode and other bulk modes, is also of theoretical interest.

Motivated by the above practical advantages and unsolved questions, a 2D topological laser was first built with a photonic crystal platform under an external magnetic field [30]. In the design of photonic crystal, InGaAsP multiple quantum wells are structured and bonded to yttrium iron garnet (YIG), a gyrotropic material grown on gadolinium gallium garnet (GGG). The topological bandgap is opened at Γ-point under static magnetic field normal to the slab, breaking the time-reversal symmetry. The gap is designed at 1.55 μm for edge mode to lase at the telecom wavelength, which is supported by the gain spectrum of InGaAsP. To confine light at the boundary of the topological cavity, another circular unit cell embedded in a hexagonal lattice with a trivial bandgap is used (Figure 6B).

A top view camera image shows edge mode emission at the interface when pumping the whole structure with a pulsed laser working at 1064 nm under the static magnetic field (Figure 6D). No edge state radiation pattern is observed without magnetic bias. To further characterize the lasing behavior, a line-defect trivial waveguide is designed close to the topological boundary to couple out the power, which is collected by a lensed fiber at the end of the waveguide. A clear lasing threshold is observed with increasing pumping power (Figure 6E). The unidirectional property of the chiral edge mode is demonstrated by flipping the direction of the static magnetic field. In Figure 6F, a reduction ratio of 11.3 dB in the emission power at the waveguide output proves the unidirectional propagation of the lasing mode. Different shapes of the topological-trivial interface are fabricated, and a similar lasing behavior is observed near the telecom wavelength. We note that the topological gap of the photonic crystal under TRS breaking is narrow (tens of pm) due to the limited magneto-optical response of YIG. Nevertheless, lasing from the topological edge mode was observed and further experimentally confirmed using second-order intensity correlation [35]. The narrow gap compared to the free spectral range for such cavities makes their design challenging but also naturally provides a mode selection mechanism. In a follow-up work, the ring-shaped topological-trivial interface is designed to generate coherent beams carrying orbital angular momentum (OAM) [35]. The device succeeds in producing

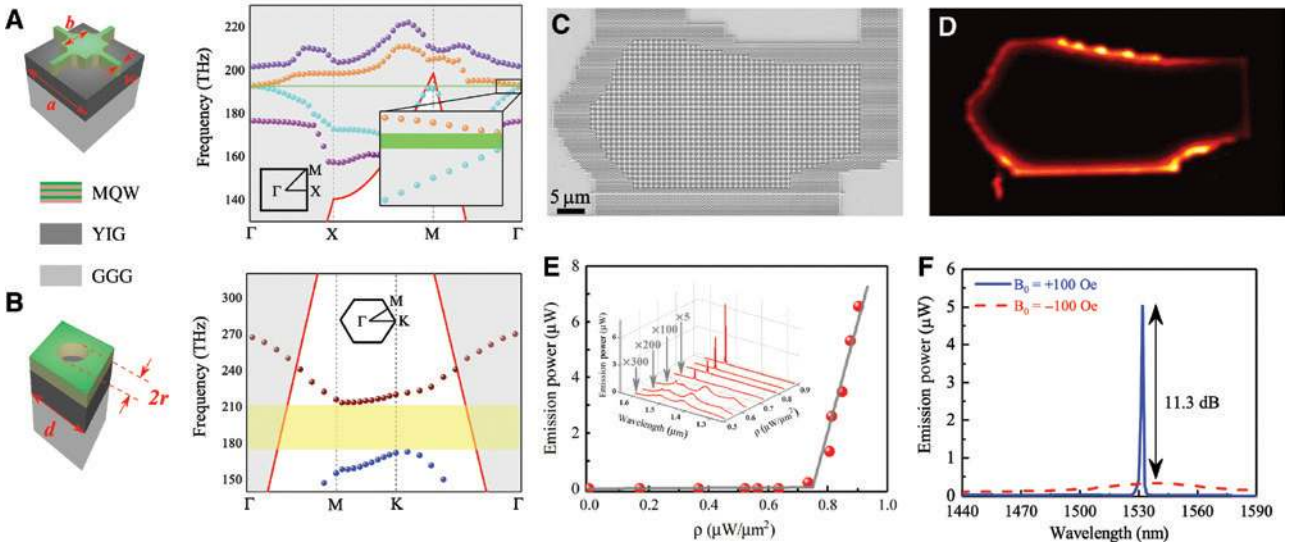

Figure 6: 2D topological photonic crystal laser with a static magnetic field.
(A,B) 3D topological (trivial) bandgap unit cell structure and corresponding band diagram. (C) SEM image of the fabricated nanostructure with topological-trivial interface in the shape of flipped US map. (D) Top lasing image of (C) under static magnetic field. (E) Emission power of the laser as a function of pumping power. (F) Output power at one end of the coupling waveguide with the opposite direction of the magnetic field normal to the structure plane (replicated from Ref. [30]).

arbitrarily large topological charge and multiplex different OAM emission onto a single sample. The ability to shape the edge mode profile hence the radiation pattern can be further optimized for communication applications. There are open opportunities for experimentally investigating such TRS-broken topological lasers toward practical applications.

Lasing from topological edge states in a 2D configuration was also studied in a lattice of microcavity polaritons [32]. The building block of microcavity polariton consists of semiconductor 2D quantum wells embedded between a pair of distributed Bragg reflectors (DBR), where the excitons are strongly coupled to the cavity modes. Polaritons are thus mixed light matter quasi-particles combining the properties of its two constituents: excitons and photons. An external magnetic field perpendicular to the 2D heterostructure leads to the Zeeman splitting of excitons, and the difference in the reflection of Bragg reflector for TE and TM wave results in the effective spin-orbit coupling of photons [74, 75]. The combination of both effects in a hexagonal microcavity polariton lattice (Figure 7A) induces a topological bandgap characterized by integer band Chern numbers [76, 78]. Hence, the time-reversal symmetry is broken, and robust chiral edge states are expected with a chirality determined by the direction of the magnetic field. Lasing in such exciton-polariton topological lattices was reported in Ref. [32] via the mode tomography of the edge states (Figure 7C). It is also worth mentioning that the gain can also be provided via electrical pumping [79].

Theoretical studies of lasing in polariton hexagonal lattices subject to an external magnetic field suggest that such states should be chiral, and significant differences between lasing in topological and trivial polariton lattices [77] should be expected. Figure 7B shows the band diagram of a stripe of the hexagonal lattice with finite size in the x-direction but infinity in the y-direction, calculated using spinor Schrodinger equations describing the time evolution of the polariton wave function. The edge mode exists at the boundary of the lattice, and the opposite group velocity indicates the unidirectional propagation. When gain is introduced in the model on one side of the edge, the eigenmode shows high amplification on that side and is expected to lase with increasing gain. The full structure of a triangular-shaped lattice with material gain along the edge is simulated for both topological (Figure 7F) and trivial (Figure 7G) designs. The trivial lasing mode is different from the topological one both in mode profile, as the trivial one only emits in one sublattice, and in the lasing spectrum [77].

In this section, we have seen that the 2D topological laser provides a novel type of light source. By breaking time-reversal symmetry with the magnetic field, it allows unidirectional propagating modes with arbitrary shape to emit. Interestingly, polariton lattices present significant nonlinearities [80], arising from the excitonic component

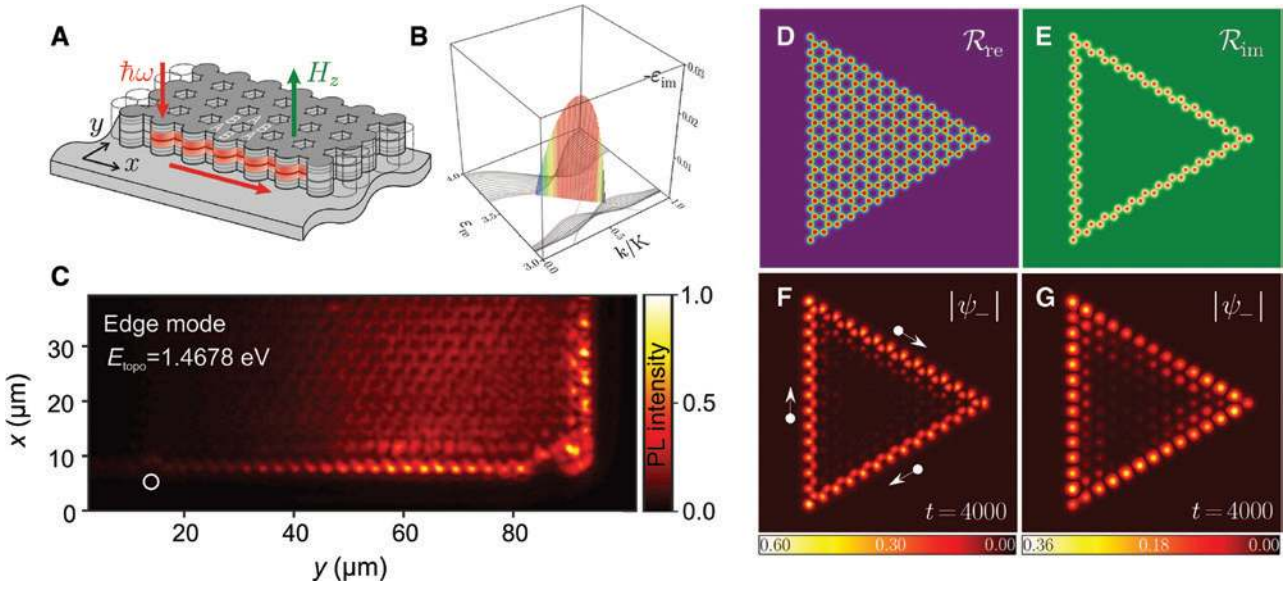

Figure 7: 2D topological polariton lasers.
(A) Scheme of polariton micropillars arranged in hexagonal shape under external magnetic field. (B) Real and imaginary part of eigenmodes for a hexagonal structure with finite-y and infinite-x size. Color bar shows that the edge mode experience amplification where $-\epsilon_{im} > 0$. All $-\epsilon_{im} < 0$ is set to zero in the plot. (C) Exciton-polariton topological edge state observed in photoluminescence experiment in the lasing regime. (D, E) Real and imaginary part of the photonic potential for a triangular-shaped lattice with the gain confined at the boundary. (F) Calculated unidirectional edge mode lasing profile under external magnetic field in the steady-state with arrows indicating the current direction. (G) Simulation of lasing from a trivial bandgap structure (zero spin-orbit coupling) where only sites in one sublattice emit ((A) Replicated from Ref. [76], (C) replicated from Ref. [32], and (B, D–G) from Ref. [77]).

of polaritons, and provide a very promising platform to study the interplay of topology and nonlinearity in the lasing regime [81, 82].

5 2D topological lasers without breaking TRS

There is another class of 2D topological lasers, which do not break the time reversal symmetry [31, 73]. The structure is based on the construction of the Harper-Hofstadter model using ring resonators originally realized by [5, 6] in a passive silicon photonics platform.

The Harper-Hofstadter model is a 2D square lattice model with a uniform constant magnetic field applied perpendicular to the 2D plane. In tight-binding models, the effect of the magnetic vector potential enters as complex hopping phases upon hopping to adjacent sites. The Hamiltonian of the Harper-Hofstadter model with the magnetic vector potential taken in the Landau gauge, $A = (0,\ Bx)$, is

$$H(B) = -J\sum_{x,y}\left[a^{\dagger}_{x+1,y}a_{x,y} + \mathrm{e}^{iBx}a^{\dagger}_{x,y+1}a_{x,y} + \mathrm{H.c.}\right]$$

where we set the lattice spacing to be unity and assumed that the hopping strength is isotropic. The phase that a particle acquires after hopping around a plaquette of the square lattice is B (see Figure 8A). When $B = 2\pi p/q$ with p and q being mutually prime integers, the model has q bands, and all the bands are topologically nontrivial unless p/q is an integer or a half-integer. The topological invariants describing the system are Chern numbers, which equal the number of modes circulating around the system due to the bulk-edge correspondence. Hafezi et al. [5, 6] realized the Harper-Hofstadter model by connecting Si microring resonators via anti-resonant link resonators, which are constructed so that the path length for photons hopping from one resonator to another is generally different from the path length hopping in the opposite direction. This path difference effectively introduces the complex hopping phase necessary to construct the Harper-Hofstadter model (see Figure 8B).

The Harper-Hofstadter model, itself, breaks the time-reversal symmetry unless B is an integer or a half-integer multiple of 2π. In the construction of Refs. [5] and [6], time reversal symmetry was indeed not broken (there is no external magnetic field). In fact, the Si microresonator supports two degenerate modes: in one of them, the

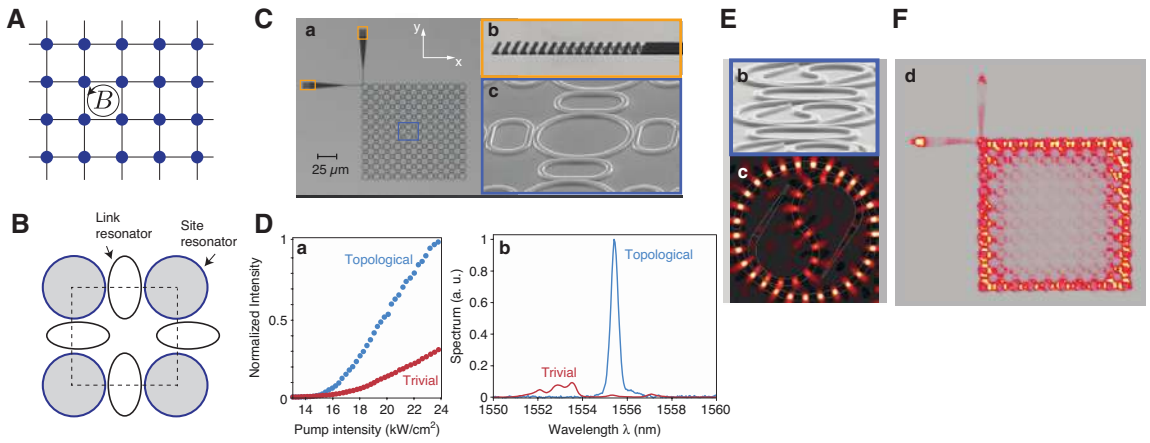

Figure 8: 2D topological microring cavity laser.
(A) A schematic picture of the Harper-Hofstadter model. A particle hopping around a plaquette of the lattice acquires a phase B. (B) How to construct a plaquette of the Harper-Hofstadter model with resonators. Site resonators are connected by link resonators, which are anti-resonant with modes of the site resonators. Link resonators connecting site resonators horizontally are positioned symmetrically with respect to hopping to right and left, whereas link resonators connecting vertical sites are asymmetrically positioned. This asymmetry introduces different optical paths for photons going up with respect to those going down, resulting in an effective hopping phase upon vertical hopping. (C) Image of the experiment of Ref. [31]. The Harper-Hofstadter model with 10×10 lattice sites are constructed. There are output couplers at the upper left corner. (D) Intensity of the emission when the perimeter of the system is pumped as a function of (a) pump intensity and (b) wavelength. (E) Resonators with S-shaped waveguides. The lower figure is the numerically calculated field distribution of a resonator with an S-shaped element. (F) Experimentally measured intensity profile of the lasing edge mode from the topological Harper-Hofstadter model made of resonators with S-shaped elements. The intensity difference in the output couplers indicate that the chiral edge state propagating in the counter-clockwise direction has much higher intensity than that propagating in the opposite direction. (C–F) Adapted from Ref. [31].

light circulates in the clockwise direction, and in the other, it circulates in the counter-clockwise direction. The clockwise mode obeys the Harper-Hofstadter model with magnetic field strength B, while the counter-clockwise mode obeys the Harper-Hofstadter model with opposite magnetic field $-B$. The time-reversal symmetry of the full system is preserved, and the overall Hamiltonian in the basis of clockwise and counter-clockwise modes, which serve as pseudospins, is then:

$$H_{\text{overall}} = \begin{pmatrix} H(B) & 0 \\ 0 & H(-B) \end{pmatrix}$$

This Hamiltonian possesses two time-reversal symmetries (anti-unitary operators, which commute with the Hamiltonian), $T_1 = \sigma_x K$ and $T_2 = \sigma_y K$, where K is complex conjugation, and the Pauli matrices act on the pseudospin basis. Note that $KH(B)K = H(-B)$. There is also an on-site pseudospin conservation symmetry $U = \sigma_z$, which is essentially the product of T_1 and T_2. As long as U is unbroken, and thus, there is no coupling between clockwise and counter-clockwise modes, the system behaves as two copies of the Harper-Hofstadter models with opposite magnetic fields. The system is thus similar to the time-reversal symmetric quantum spin-Hall Hamiltonian in electronic systems [83–85]. However, it is worth mentioning the difference between the time-reversal symmetric quantum spin-Hall systems of electrons and its photonic analog. The model with unbroken U possesses both bosonic and fermionic time-reversal symmetries because $T_1^2 = +1$ and $T_2^2 = -1$. In electronic quantum spin-Hall systems, one can allow perturbations mixing two spins, which break U and T_1 but not T_2, and the resulting model is described by the Z_2 topological invariant characteristic of two-dimensional fermionic systems with time-reversal symmetry [83]. On the other hand, in bosonic systems such as photonics, time-reversal invariant perturbations will, in general, mix two pseudospins and break U and T_2 but not T_1, which renders the symmetry class of the model AI in the 10-fold way classification of topological insulators and superconductors, which is topologically trivial in two dimensions [86, 87]. This implies that the topological features of the model are protected as long as the pseudospin conservation is obeyed. The experiment of [5, 6] observed negligible backscattering, and hence, the system is well described as two decoupled copies of the Harper-Hofstadter models with opposite magnetic fields.

The authors of Ref. [31] used ring resonators made of InGaAsP, a material with optical gain, and constructed the Harper-Hofstadter model with $B = 2\pi/4$. Resonators are

made of waveguides, which operate at a wavelength of 1550 nm. See Figure 8C for the images of the experiment. To obtain lasing at topological edge states, the authors of Ref. [31] added gain only to the perimeter of the system; in this way, the overlap of the gain profile with the topological edge state becomes much larger than that with the bulk states, and the topological lasing is preferred [73]. Figure 8D shows the comparison of lasing between the topological Harper-Hofstadter model with $B=2\pi/4$ and a simple square lattice, which is topologically trivial. For both topologically trivial and nontrivial cases, only the perimeter of the system is pumped. The authors found that the lasing is much more efficient for the topological case. Emission spectrum has only one peak for a topological case, whereas the trivial case has a much broader emission spectrum. The broad emission spectrum for the trivial case is attributed to fragmented lasing at several different segments of the perimeter, where localized modes exist due to intrinsic disorders present in the system. On the other hand, the lasing of the topological case occurs from topological edge states, which are extended around the entire perimeter of the system, and thus, no fragmentation of lasing is observed. The authors of Ref. [31] further studied the propagating nature of lasing from the topological edge states. By pumping only a part of the perimeter of the system and observing the emission at output couplers situated at a corner of the system, they observed that lasing from topological edge states propagate and reach the output coupler much more than lasing from the perimeter of the trivial model. The topological lasing from propagating topological edge states has advantages that the entire edge can participate in lasing from a single mode due to the extended nature of the edge states. Such single-mode topological lasing is robust even against disorders at edges. Single-mode lasing and robustness against disorders are confirmed in the experiment of Ref. [31]. Nevertheless, further and careful investigations are necessary to clarify the potential of practical use of this type of topological lasers. One concern is its narrow topological bandgap (less than 1 nm), which is comparable to that of the laser linewidth (full width) well above the threshold. The stability of such laser device under harsh environments should be investigated further.

Lasing in propagating topological edge states of the Harper-Hofstadter model has also been theoretically studied in Refs. [88] and [89]. The authors of Ref. [88] found that pumping only a part of the edge has higher lasing threshold compared to the case where the entire edge is pumped. When only a part of the edge is pumped, even when exponential growth of an initial perturbation starts to happen, the amplified region travels away from the pumping region due to nonzero group velocity of chiral edge states, and the amplitudes decay back to zero; such form of instability is called *convective instability*. In order to achieve *absolute instability* and stable lasing, higher lasing threshold is required. The authors of Ref. [88] also found that topological lasing from pumping only a part of the edge is much less robust against disorders compared to the case where the entire edge is pumped.

When the time-reversal symmetry is not broken, there are two degenerate topological edge states, one made of clockwise modes and the other made of counter-clockwise modes. These constitute helical edge states of the system. In the experiment, lasing can therefore occur from both helical edge states. To break the time-reversal symmetry, the authors of Ref. [31] also constructed the Harper-Hofstadter lattice made of S-shaped resonators (see Figure 8E). The spatial asymmetry of the S-shape combined with nonlinearity/loss leads to lasing in a particular mode, achieving lasing in topological edge states propagating only in one direction (see Figure 8F).

6 Non-Hermiticity-based photonic topological effects

Because practical optical cavities (waveguides) are open dissipative systems and lasers (modulators) utilize amplification (absorption), photonic devices can be understood as a semi-classical analogy of non-Hermitian quantum systems [90]—they do not preserve the number of photons. Uniform optical gain or loss just adds an offset imaginary term to the eigenspectrum for the original Hermitian system. Thus, topological lasers with homogeneous or gently distributed pumping essentially take over the topological properties of their underlying Hermitian structure. Many of the aforementioned examples in this article fall in to this category of *pumped Hermitian topological systems*.

On the other hand, specific non-Hermiticity, e.g. alternating gain and loss and asymmetric couplings, was recently found to trigger unconventional topological functionalities, concepts, and phenomena, such as reconfigurable topological insulating phases by gain and loss, extended classification of symmetry-protected topological phases, new types of bandgaps and emergent topological features, and modified bulk-boundary correspondence, etc. Extensive theoretical investigations on these topics have been proceeding, and photonic technology will play a pivotal role in opening up this new arena, as it did in the field of non-Hermitian or parity-time- (PT-) symmetric optics [91–95].

This section briefly overviews the recent progress in non-Hermitian topological physics and photonics, so that it hopefully enhances photonics research into this exciting direction.

6.1 The complex SSH model

Studies on the impact of non-Hermiticity on topological photonics branched off from the trend of exploring PT-symmetric photonic devices. The seminal work by Schomerus [49] studied the 1D photonic SSH model [96] with staggered on-site gain and loss, called complex SSH model (Figure 9A),

$$H_{cSSH}(k)=\begin{pmatrix} -i\gamma & \eta+\kappa e^{-ika} \\ \eta+\kappa e^{ika} & i\gamma \end{pmatrix},$$

where k is the Bloch wavenumber, γ is the magnitude of gain ($i\gamma$) and loss ($-i\gamma$) rate, a is the spatial period of the unit cells, and η and $\kappa \in \mathbb{R}$ are the distinct cavity couplings determined by their alternating spatial intervals. Here, it was shown theoretically that a topological defect state was feasible (Figure 9B and C), regardless of the following peculiar features of the system. First, the topological edge and defect states have finite imaginary eigenvalues (Figure 9B), namely, net gain or loss in their dynamics [97, 98]. Second, the conventional Zak phase [99] becomes continuous then fails to be a good topological number of this non-Hermitian system [100, 101]. Moreover, as seen in the system eigendetuning, $\Delta\omega_{cSSH}(k)=\pm\sqrt{\kappa^2+\eta^2+2\eta\kappa\cos(ka)-\gamma^2}$, the bandgap in the real part of frequency (frequency bandgap) closes for $|\gamma|>|\kappa-\eta|$ with an exceptional point (EP), i.e. non-Hermitian degeneracy at a defective point (Figure 9D). Here, the bulk eigenstates crossing an EP undergo a transition from distributed modes to localized modes (PT symmetry breaking). With a finite frequency gap remaining in the system, the relevant topological states are experimentally observable, even though they have finite net gain or loss [44, 46, 102].

In the complex SSH system with open boundaries, the topological edge states undergo the PT symmetry breaking independent of that of the bulk modes. Thus, as shown in Section 2, one of the robust edge states can be configured to be the only mode that obtains net gain, suppressing the mode competition in lasing [25, 27] (Figure 3). Moreover, although small finite SSH lattices exhibit non-negligible frequency (propagation constant) splitting between the weakly coupled edge states, the gain and loss can cancel it and give the exact zero modes at the resultant EP [103].

6.2 Gain- and loss-induced photonic topological insulating phase

Particular interest in non-Hermitian topological photonics is on new functionalities and phenomena that have

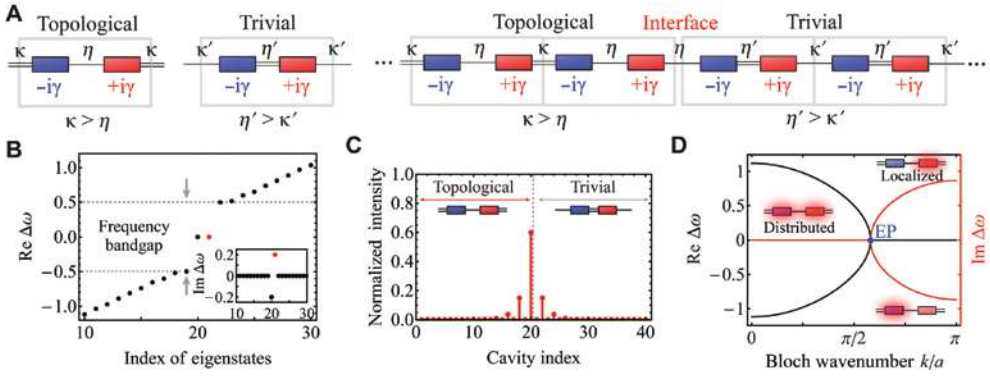

Figure 9: The complex SSH model [49], where staggered imaginary potential is applied to the system of periodic optical dimers based on two alternating couplings κ and η.
Here, κ and η is determined by the system structure, i.e., distinct spatial intervals between the cavities. (A) Left: the topologically nontrivial and trivial unit cells. Right: a junction between the topological and trivial lattices with opposite magnitude relations of the couplings. The system forms a robust topological defect state on the interface. (B) Eigenfrequency spectrum $\Delta\omega$ of the system with the junction shown in (A) and 20 cavities for each of the topological and trivial parts. $\kappa=\eta'=1$, $\eta=\kappa'=0.5$, $\gamma=0.2$. The red dots show the complex eigenfrequency of the topological defect state. The other zero mode is the edge state of the topological lattice. (C) Intensity distribution of the topological defect state. (D) Band structure with large gain and loss. $\kappa=1$, $\eta=0.5$, $\gamma=1$. The gain and loss makes the bandgap close and form an EP. The eigenmodes with imaginary detuning beyond the EP are localized at either of the cavity with gain or that with loss.

no counterparts in Hermitian systems. From the technical viewpoint, it is common to control effective on-site imaginary potential in optical devices, i.e. gain and loss in lasers, amplifiers, and modulators. Such an operation can also be fast, effective, and local compared to the handling of the real part of the refractive index, which needs intrinsically small optical nonlinear or electro-optic effects. However, conventional Hermitian topological optical devices rely mostly on their built-in structures and magneto-optical effects for their nontrivial photonic topology [16–18, 21]. Thus, it is a technical challenge to achieve fine-grained control of the topology and resultant features such as the number and position of robust topological edge states, after the devices are fabricated. If there is a scheme to manipulate photonic topology only with gain and loss (via pumping), topological photonic modes, which are robust to structural fluctuation inevitable in tiny devices, can be incorporated in a suite of element technology for reconfigurable optical circuits.

A simple and unique scheme to enable the idea in 1D coupled cavities (and waveguides) was proposed in Ref. [104]. In the complex SSH model initially studied, the difference of imaginary potential in the unit cell can close but not open the frequency bandgap. Thus, it can break but not produce the topological insulating phase. In contrast, the proposed method [104] prepares a linear cavity array with uniform couplings (κ) as a system with identical four-cavity periods (Figure 10A). Here, gain is introduced to two sequential cavities; loss is applied to the other two, and they are balanced under two magnitudes (g_1 and g_2) so that the system's effective Bloch Hamiltonian is given by,

$$H_{TN}(k)=\begin{pmatrix} ig_1 & \kappa & 0 & \kappa e^{-ika} \\ \kappa & -ig_2 & \kappa & 0 \\ 0 & \kappa & -ig_1 & \kappa \\ \kappa e^{ika} & 0 & \kappa & ig_2 \end{pmatrix}.$$

In this condition, gain and loss can induce the frequency bandgap and even a transition between topological and trivial photonic insulating phases.

Effective dimerization by the cavities with gain and loss can be understood as the physical mechanism of the peculiar topological property. As mentioned above, the contrast of on-site imaginary potential can cancel the

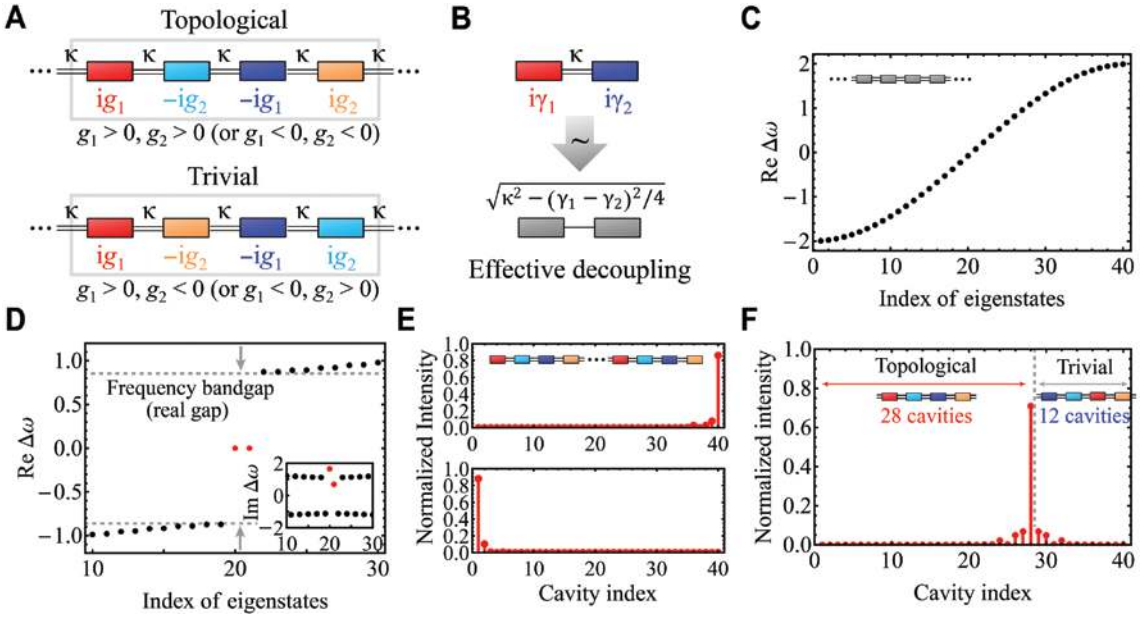

Figure 10: Gain- and loss-induced 1D photonic topological insulating phase [104].
(A) Four-cavity unit cell of the model. Top and bottom: topologically nontrivial and trivial systems, respectively. (B) Reduction of frequency splitting of supermodes by the contrast of imaginary potential. It works as effective decoupling that is especially enhanced when the signed magnitudes γ_1 and γ_2 have opposite signs (i.e., the cavities have gain and loss). (C) Eigendetuning of the system of 40 cavities with open ends and no gain or loss. It traces the system band structure that is gapless and cosinusoidal. $\kappa=1$. (D) Complex eigendetuning profile of the same lattice with the gain and loss introduced, so that the system becomes topologically nontrivial. It has a bandgap in Re$\Delta\omega$ (real gap), and the red dots correspond to the topological edge states. $\kappa=1$, $g_1=2$, $g_2=1$. (E) Intensity distributions of the edge states in (D). Each of them localizes at each edge of the lattice. (F) A topological defect state formed at the interface between topological and trivial parts in a single cavity array. Their photonic topology depends solely on the gain and loss; thus, the position and number of such topological states can be controlled by the pumping profile of the system.

splitting of the eigenvalues and result in the transition to the localization of eigenstates [105]. In the system of the four-cavity periods (Figure 10A), while the couplings between the cavities with gain and those with loss are effectively suppressed (Figure 10B), both the two cavities with gain and those with loss remain bound. As a result, despite that the Hermitian system without gain or loss ($g_1 = g_2 = 0$) gives gapless dispersion (Figure 10C), the non-Hermitian unit cell (g_1, $g_2 \neq 0$) behaves as a pair of dimers, which leads to the frequency bandgap (Figure 10D). In addition, the array exhibits the topological insulating phase with a couple of midgap edge states, if the cavities with gain (or loss) are located separately at the both ends of the unit cell ($g_1 g_2 > 0$). Otherwise, the system is in the topologically trivial phase that results in no topological state ($g_1 g_2 < 0$). The topological transition of this single-gap non-Hermitian system can be confirmed by the discrete change in the non-Abelian global Berry phase (total complex Berry phase) with the biorthogonal basis [106]. The photonic topology is based on a non-Hermitian symmetry called pseudo-anti-Hermiticity, $\Gamma H_{TN}^{\dagger}(k)\Gamma^{-1} = -H_{TN}(k)$, where $\Gamma = \Gamma^{-1} = I_2 \otimes \sigma_z = \mathrm{diag}\,(1, -1, 1, -1)$ here [107, 108]. Thus, as long as the cavity coupling is reciprocal, $\mathrm{Re}\Delta\omega = 0$ of the edge states is protected against fluctuation of all the parameters in the model, κ, g_1, and g_2. Topological winding of the bulk coupling parameters of $H_{TN}(k)$ around $\mathrm{Re}\Delta\omega = 0$ can also be visualized.

The gain- and loss-based topological array has a pair of topological edge states, each of which localizes at each edge due to parity symmetry breaking (Figure 10E). In addition, by the electrically or optically tuned pumping for every cavity, which is feasible in on-chip laser systems [25–27, 30, 34, 109, 110], it is possible to introduce both topological and trivial insulating parts with their sizes and position manipulated freely in a single array. As a result, topological defect states, formed at every interface between the two distinct parts, are controlled accordingly (Figure 10F). It is noteworthy that the reconfigurable photonic topology can be temporally handled and compatible with recent approaches that embed wave topology in the system dynamics itself [111, 112]. The scheme was also extended to a second (higher) order non-Hermitian topological insulator, which exhibits degenerate topological corner states in a 2D system [113]. It would further inspire the gain- and loss-based topology for 2D and 3D non-Hermitian systems, which is already been under intense research [114–122]. A systematic technique to construct topological tight-binding models [123] might be extended and applied to non-Hermitian Hamiltonians.

It can be emphasized that the band engineering with gain and loss here offers a new avenue for accessing a non-Hermitian topological insulating phase controlled solely by non-Hermitian degrees of freedom, in contrast to the complex SSH model.

6.3 Classification of symmetry-protected non-Hermitian topological phases

Recently, systematic classifications of symmetry-protected non-Hermitian topological systems appeared [124–126]. Among the literature, a consistent framework by Kawabata et al. [125] points out that, due to the inequality of the transpose and complex conjugate of non-Hermitian single-particle Hamiltonian, $H^{\mathrm{T}} \neq H^{*}$, some symmetries that were regarded equivalent ramify, and some thought distinct are unified as well [118]. In short, Ref. [125] redefines Altland-Zirnbauer (AZ) symmetry classes [127] as ones comprising the conventional time-reversal symmetry (TRS) and particle-hole symmetry (PHS), which those of second-quantized systems originally reduce to:

$$T_{+}H^{*}(\boldsymbol{k})T_{+}^{-1} = H(-\boldsymbol{k}), \qquad T_{+}T_{+}^{*} = \pm 1\ (\mathrm{TRS}),$$

$$C_{-}H^{\mathrm{T}}(\boldsymbol{k})C_{-}^{-1} = -H(-\boldsymbol{k}), \qquad C_{-}C_{-}^{*} = \pm 1\ (\mathrm{PRS}),$$

where T_{+} and C_{-} are unitary matrices. On the other hand, their dual counterparts with H^{T} and H^{*} switched should be treated distinctly as *variant* symmetries, denoted by TRS† and PRS†:

$$C_{+}H^{\mathrm{T}}(\boldsymbol{k})C_{+}^{-1} = H(-\boldsymbol{k}), \qquad C_{+}C_{+}^{*} = \pm 1\,(\mathrm{TRS}^{\dagger}),$$

$$T_{-}H^{*}(\boldsymbol{k})T_{-}^{-1} = -H(-\boldsymbol{k}), \qquad T_{-}T_{-}^{*} = \pm 1\,(\mathrm{PRS}^{\dagger}),$$

and they form another set of symmetry classes named AZ† symmetry. Here, non-Hermitian chiral symmetry (NH CS), based on the combination of each pair of symmetries, is described in the common form as:

$$\Gamma H^{\dagger}(\boldsymbol{k})\Gamma^{-1} = -H(\boldsymbol{k}), \qquad \Gamma^{2} = 1\,(\mathrm{NH\ CS}).$$

Finally, sub-lattice symmetry (SLS) hence gets separate from CS as

$$SH(\boldsymbol{k})S^{-1} = -H(\boldsymbol{k}), \qquad S^{2} = 1\,(\mathrm{SLS}).$$

With all of them considered, the classification becomes 38-fold in non-Hermitian physics, indicating significant extension from the celebrated 10-fold way [86, 128] for Hermitian topological insulators and superconductors [129, 130]. Note that NH CS is equivalent to pseudo-anti Hermiticity. Remarkably, it is distinct from the prevalent form of (Hermitian) chiral symmetry, $\Gamma H(\boldsymbol{k})\Gamma^{-1} = -H(\boldsymbol{k})$.

Photonic systems with imaginary on-site potential all satisfy $H^T \neq H^*$, and they hence break TRS in most cases. Thus, it is reasonable to start with checking the list of A, AIII, and AZ† symmetry classes for classifying such systems. For example, the complex SSH model is in the AIII class of the non-Hermitian version (Complex AIII) characterized by NH CS [125]. The abovementioned four-cavity model $H_{TN}(k)$ [104] actually respects TRS† with $C_+ = I_4 = \mathrm{diag}(1, 1, 1, 1)$, PRS† with $T_- = \mathrm{diag}\,(1, -1, 1, -1)$, and hence NH CS with $\Gamma = T_-$. Thus, in terms of symmetry, it is classified into an unconventional class named BDI†. It can nonetheless be interpreted as Complex AIII due to the criticality of NH CS on the topology as well, and the two classes are equivalent in 1D. The theory [125] tells that when the system has a "real gap," meaning exactly the same as frequency bandgap here, it is characterized by an integer ($\mathbb{Z}$) index. This supports the correspondence between the edge states and global Berry phase of the non-Hermiticity-based topologically insulating lattice. Applying the encompassing table of non-Hermitian symmetries will promote further the understanding of non-Hermitian topological insulating systems and help with their systematic design.

Here, PT symmetry in the bulk complex SSH system, i.e. $\sigma_x H^*_{cSSH}(k)\sigma_x = H_{cSSH}(k)$, does not affect the topological invariant and edge states under the frequency gap, provided by NH CS. Instead, it protects the system from the "non-Hermitian skin effect" mentioned later, where the bulk modes concentrate over an edge via non-Hermiticity [125].

6.4 Complex bandgap and emergent non-Hermitian topological effects

Another important fact in non-Hermitian physics is that it is necessary to redefine the *bandgap* because eigenspectra of non-Hermitian systems are generally complex [115, 125, 131]. One of the two possible types of "complex bandgaps" is called a *line gap* and defined as a line-shaped blank of eigenstates in the bulk spectrum plotted on the complex plane (Figure 11A). The other is termed a *point gap*, which means a (symmetry-protected) frequency point that the spectrum does not cross (except for the case of no symmetry) (Figure 11B). Line gaps are divided further into two, and one is the forementioned real gap indicating the discontinuity in the real part of eigenfrequencies (i.e. the line gap parallel to the imaginary axis). The other is the absence of states for a range of their imaginary part, called an imaginary gap. A remarkable point is that possible system topological indices also depend on which complex gap the system possesses [125].

A topological structure specific to non-Hermitian systems shows up, especially when their complex spectra

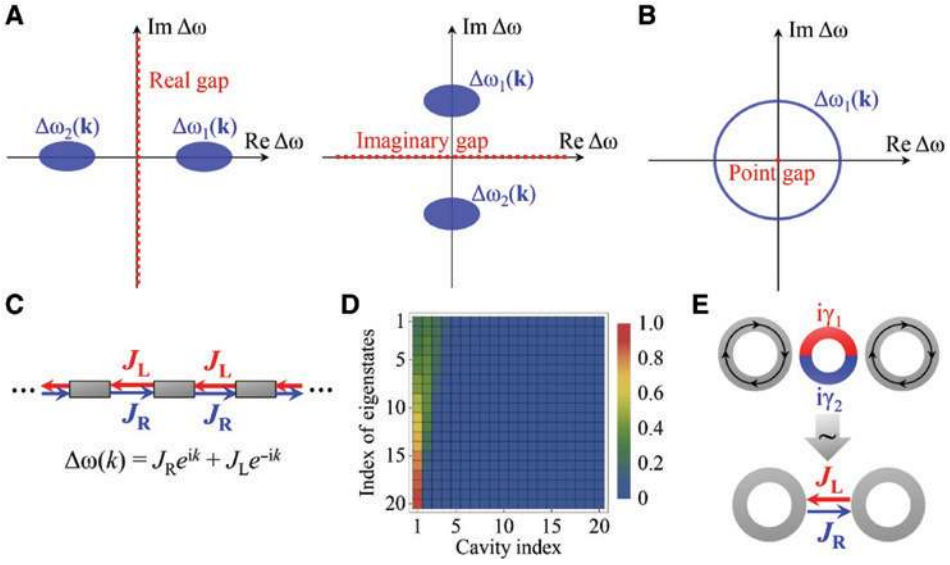

Figure 11: Complex bandgaps and non-Hermitian skin effect.
(A, B) Definitions of the complex bandgap. (A) Line gap, where the bulk bands $\Delta\omega_1$(k) and $\Delta\omega_2$(k) do not cross a certain line in the complex plane. Left: line gap in terms of Re$\Delta\omega$ (real gap). Right: that in Im$\Delta\omega$ (imaginary gap). (B) Point gap, where the eigenvalues do not touch a certain (symmetry-protected) point in the plane. (C) Fundamental 1D lattice with asymmetric hopping ($J_L > J_R$ here), which exhibits a point gap [131]. (D) Normalized intensity distributions of all the right eigenvectors for a system of 20 cavities with the asymmetric couplings. $J_L = 3$, $J_R = 1$. All the eigenmodes localize around the left edge due to $J_L > J_R$(non-Hermitian skin effect). (E) Possible realization of asymmetric hopping in a coupled ring cavity system [132, 133]. The ancillary ring with distributed gain and loss (center) induces imaginary gauge fields (effective directional amplification and attenuation) for a supermode with a specific chirality.

form loops around point gaps [131]. In this case, the system is characterized by the geometric charge not of eigenstates but rather of the band spectrum $H(\boldsymbol{k})$ for a certain loop in the k space: $w_n = 1/(2\pi)\oint \mathrm{d}k\, \partial_k \arg H_n(\boldsymbol{k})$, where n is the eigenstate index and $H_n(\boldsymbol{k})$ is the nth eigenfrequency. The non-Hermitian winding number w here is considered as the sum or difference of $\{w_n\}$ among distinct states and called vorticity [114, 115, 131]. In one dimension, at least, systems with point gaps and finite w are closely related to lattices with asymmetric hopping (Figure 11C). The pioneering work reports that such a system can have edge states, but they can be dynamical and unstable [131].

It is also known that non-Hermiticity can explicitly disrupt the conventional bulk-boundary correspondence (BBC) held in Hermitian systems [121, 134–145]. Especially, asymmetric couplings make not only topological edge states but also non-topological bulk states localize around an either end to which the stronger hopping is directed (non-Hermitian skin effect) (Figure 11D). Regarding *line-gapped* systems, the topological transition in this case is explained by the winding number of the Q matrix based on the biorthogonal projection operator [136, 139, 140]. Furthermore, imaginary gauge fields [132, 133, 142, 146], which indicate paired effective amplification in one way and attenuation to the other, are presented as an intelligible interpretation of these anomalous properties. The skin effect will hence stem from some symmetry breaking induced by non-Hermiticity [142, 147]. General complex asymmetric (directional) couplings can break inversion symmetry and all the elemental symmetries ($\mathrm{TRS}^{(\dagger)}$ and $\mathrm{PRS}^{(\dagger)}$) for the AZ and $\mathrm{AZ}^{\dagger}$ classes. A latest study [148] points that the skin effect is unavoidable in *point-gap* topology. Moreover, once it occurs in any systems with open boundaries, covering most of its experimental realizations, it inevitably closes the bulk point gap and washes out the relevant topological protection of the boundary modes. The work shows a new way to circumvent the collapse of BBC via a peculiar skin effect retaining $\mathrm{TRS}^{\dagger}$.

For the purely 1D optical lattice comprising single-mode elements, the directional hopping means non-reciprocity, and the foregoing anomaly is hence considered unrealizable as a static response of standard dielectric devices. Meanwhile, ring cavity arrays with ancillary components are proposed to induce imaginary gauge fields in supermodes with a specific chirality (Figure 11E) [114, 132, 133].

Finally, it is noteworthy that exceptional points (EPs) [93–95, 149–155], i.e. defective complex-gap closings, will be classified separately [156]. They can also be symmetry protected [157–159] and are featured by topological indices that can lead to topological states. The topological classification of EPs suggests that some robust photonic defect states in early reports would be EP-based [114, 160, 161]. With a certain range of parameters, the four-cavity model $H_{TN}(k)$ can also have a couple of EPs (point-gap closings) on $\mathrm{Re}\Delta\omega = 0$, which are protected by NH CS and separated by the imaginary gap. These EPs have distinct fractional charge vortices $w_n = \pm 1/2$ and can hence lead to edge states in the system with the real gap closed. Technically, however, some gaps are still to be filled for the comprehensive understanding of the BBC in systems with EPs. On the experimental side (right), eigenstates of non-Hermitian systems are generally non-orthogonal, and photonic states with the same real frequency, which especially center at EPs, can hence couple to each other. Thus, cares might be taken to selectively control topological states in non-Hermitian optical systems. Meanwhile, recent judicious demonstration [25, 27, 44, 46, 102, 162, 163], which is reaching controlled light steering in a 2D lattice [164], suggests a bright outlook on applying the series of novel non-Hermitian topological properties for future photonic circuits.

7 Summary

In this paper, we reviewed recent progress in active topological photonics. We particularly discussed topological lasers and non-Hermitian topological physics enabled by gain and loss. We reviewed that various combinations of topological photonic modes with semiconductor gain were experimentally implemented to realize different types of topological lasers, some properties of which are topologically protected. These prototypical devices point directions for the development of novel lasers with advanced features, such as robust operation under harsh environmental conditions as well as in tightly limited spaces, unidirectional light output immune to back-reflection noise, and electron-spin-controllable lasing. The exciting physics in topological photonic systems with gain and loss will arguably result in fascinating ideas for further advancing photonic devices. Such non-Hermitian topological photonic systems also offer abundant opportunities to explore novel physics that may be difficult to access using conventional experimental tools in condense matter physics. The field of active topological photonics has just begun and will rapidly grow in the realm of both practical photonic device engineering and fundamental physics.

Acknowledgments: The authors thank K. Kawabata, The University of Tokyo, for fruitful discussions and M. Parto, D.N. Christodoulides and M. Khajavikhan for providing a schematic illustration. Y.O., Y.A., and S.I. thank MEXT KAKENHI Grant Number JP15H05700,

JP15H05868, and 17H06138, Funder Id: http://dx.doi.org/10.13039/501100001691, and New Energy and Industrial Technology Development Organization (NEDO). Y.O., T.O., and S.I. thank JST CREST Grant Number JPMJCR19T1, Funder Id: http://dx.doi.org/10.13039/501100003382. K.T. and M.N. acknowledge JST CREST under Grant Number JPMJCR15N4, Funder Id: http://dx.doi.org/10.13039/501100003382. T.O. is supported by JSPS KAKENHI Grant Number JP18H05857, Funder Id: http://dx.doi.org/10.13039/501100001691, JST PRESTO Grant Number JPMJPR19L2, Funder Id: http://dx.doi.org/10.13039/501100009023, RIKEN Incentive Research Project, and the Interdisciplinary Theoretical and Mathematical Sciences Program (iTHEMS) at RIKEN. A.A. acknowledges support from the H2020-FETFLAG project PhoQus (820392, Funder Id: http://dx.doi.org/10.13039/501100000780), the QUANTERA project Interpol (ANR-QUAN-0003-05, Funder Id: http://dx.doi.org/10.13039/501100000780), the French National Research Agency project Quantum Fluids of Light (ANR-16-CE30-0021, Funder Id: http://dx.doi.org/10.13039/501100001665), the French government through the Programme Investissement d'Avenir (I-SITE ULNE/ANR-16-IDEX-0004 ULNE), and the Métropole Européenne de Lille (MEL) via the project TFlight. B.K. acknowledges the Office of Naval Research Young Investigator Award N00014-17-1-2671, Funder Id: http://dx.doi.org/10.13039/100000006 and NSF Career Award ECCS-1554021, Funder Id: http://dx.doi.org/10.13039/100000001, Funder Id: http://dx.doi.org/10.13039/100000001.

References

[1] Haldane FDM, Raghu S. Possible realization of directional optical waveguides in photonic crystals with broken time-reversal symmetry. Phys Rev Lett 2008;100:013904.
[2] Raghu S, Haldane FDM. Analogs of quantum-Hall-effect edge states in photonic crystals. Phys Rev A 2008;78:033834.
[3] Wang Z, Chong Y, Joannopoulos JD, Soljačić M. Observation of unidirectional backscattering-immune topological electromagnetic states. Nature 2009;461:772–5.
[4] Rechtsman MC, Zeuner JM, Plotnik Y, et al. Photonic Floquet topological insulators. Nature 2013;496:196–200.
[5] Hafezi M, Demler EA, Lukin MD, Taylor JM. Robust optical delay lines with topological protection. Nat Phys 2011;7:907–12.
[6] Hafezi M, Mittal S, Fan J, Migdall A, Taylor JM. Imaging topological edge states in silicon photonics. Nat Photonics 2013;7:1001–5.
[7] Khanikaev AB, Mousavi SH, Tse W-K, Kargarian M, MacDonald AH, Shvets G. Photonic topological insulators. Nat Mater 2013;12:233–9.
[8] Chen W-J, Jiang S-J, Chen X-D, et al. Experimental realization of photonic topological insulator in a uniaxial metacrystal waveguide. Nat Commun 2014;5:5782.
[9] Wu L-H, Hu X. Scheme for achieving a topological photonic crystal by using dielectric material. Phys Rev Lett 2015;114:223901.
[10] Yves S, Fleury R, Berthelot T, Fink M, Lemoult F, Lerosey G. Crystalline metamaterials for topological properties at subwavelength scales. Nat Commun 2017;8:16023.
[11] Barik S, Karasahin A, Flower C, et al. A topological quantum optics interface. Science 2018;359:666–8.
[12] Yang Y, Xu YF, Xu T, et al. Visualization of a unidirectional electromagnetic waveguide using topological photonic crystals made of dielectric materials. Phys Rev Lett 2018;120:217401.
[13] Ma T, Shvets G. All-Si valley-Hall photonic topological insulator. New J Phys 2016;18:025012.
[14] Gao F, Xue H, Yang Z, et al. Topologically protected refraction of robust kink states in valley photonic crystals. Nat Phys 2018;14:140–4.
[15] Noh J, Huang S, Chen KP, Rechtsman MC. Observation of photonic topological valley hall edge states. Phys Rev Lett 2018;120:63902.
[16] Lu L, Joannopoulos JD, Soljačić M. Topological photonics. Nat Photonics 2014;8:821–9.
[17] Lu L, Joannopoulos JD, Soljačić M. Topological states in photonic systems. Nat Phys 2016;12:626–9.
[18] Khanikaev AB, Shvets G. Two-dimensional topological photonics. Nat Photonics 2017;11:763–73.
[19] Sun XC, He C, Liu XP, Lu MH, Zhu SN, Chen YF. Two-dimensional topological photonic systems. Prog Quantum Electron 2017;55:52–73.
[20] Wu Y, Li C, Hu X, Ao Y, Zhao Y, Gong Q. Applications of topological photonics in integrated photonic devices. Adv Opt Mater 2017;5:1700357.
[21] Ozawa T, Price HM, Amo A. Topological photonics. Rev Mod Phys 2019;91:015006.
[22] Rider MS, Palmer SJ, Pocock SR, Xiao X, Arroyo Huidobro P, Giannini V. A perspective on topological nanophotonics: current status and future challenges. J Appl Phys 2019;125:120901.
[23] Simanova D, Leykam D, Chong Y, Kishvar Y. Nonlinear topological photonics. arXiv:1912.01784. https://arxiv.org/abs/1912.01784.
[24] Foa Torres LEF. Perspective on topological states of non-Hermitian systems. J Phys Mater 2020;3:014002.
[25] Parto M, Wittek S, Hodaei H, et al. Edge-mode lasing in 1D topological active arrays. Phys Rev Lett 2018;120:113901.
[26] St-Jean P, Goblot V, Galopin E, et al. Lasing in topological edge states of a one-dimensional lattice. Nat Photonics 2017;11:651–6.
[27] Zhao H, Miao P, Teimourpour MH, et al. Topological hybrid silicon microlasers. Nat Commun 2018;9:981.
[28] Han C, Lee M, Callard S, Seassal C, Jeon H. Lasing at topological edge states in a photonic crystal L3 nanocavity dimer array. Light Sci Appl 2019;8:40.
[29] Ota Y, Katsumi R, Watanabe K, Iwamoto S, Arakawa Y. Topological photonic crystal nanocavity laser. Commun Phys 2018;1:86.
[30] Bahari B, Ndao A, Vallini F, El Amili A, Fainman Y, Kanté B. Nonreciprocal lasing in topological cavities of arbitrary geometries. Science 2017;358:636–40.
[31] Bandres MA, Wittek S, Harari G, et al. Topological insulator laser: experiments. Science 2018;359:4005.
[32] Klembt S, Harder TH, Egorov OA, et al. Exciton-polariton topological insulator. Nature 2018;562:552–6.

[33] Miao P, Zhang Z, Sun J, et al. Orbital angular momentum microlaser. Science 2016;353:464–7.
[34] Carlon Zambon N, St-Jean P, Milićević M, et al. Optically controlling the emission chirality of microlasers. Nat Photonics 2019;13:283–8.
[35] Bahari B, Hsu L-Y, Pan SH, et al. Topological lasers generating and multiplexing topological light. 2019. arXiv: 1904.11873. https://arxiv.org/abs/1904.11873.
[36] Söllner I, Mahmoodian S, Hansen SL, et al. Deterministic photon–emitter coupling in chiral photonic circuits. Nat Nanotechnol 2015;10:775–8.
[37] Blanco-Redondo A, Bell B, Oren D, Eggleton BJ, Segev M. Topological protection of biphoton states. Science 2018;362:568–71.
[38] Mittal S, Goldschmidt EA, Hafezi M. A topological source of quantum light. Nature 2018;561:502–6.
[39] Fang K, Yu Z, Fan S. Realizing effective magnetic field for photons by controlling the phase of dynamic modulation. Nat Photonics 2012;6:782–7.
[40] Yuan L, Lin Q, Xiao M, Fan S. Synthetic dimension in photonics. Optica 2018;5:1396–405.
[41] Ozawa T, Price HM. Topological quantum matter in synthetic dimensions. Nat Rev Phys 2019;1:349–57.
[42] Asbóth JK, Oroszlány L, Pályi A. A short course on topological insulators, lecture notes in physics, Vol. 919. Cham, Switzerland, Springer International Publishing, 2016.
[43] Delplace P, Ullmo D, Montambaux G. Zak phase and the existence of edge states in graphene. Phys Rev B 2011;84:195452.
[44] Zeuner JM, Rechtsman MC, Plotnik Y, et al. Observation of a topological transition in the bulk of a non-hermitian system. Phys Rev Lett 2015;115:040402.
[45] Blanco-Redondo A, Andonegui I, Collins MJ, et al. Topological optical waveguiding in silicon and the transition between topological and trivial defect states. Phys Rev Lett 2016;116:163901.
[46] Poli C, Bellec M, Kuhl U, Mortessagne F, Schomerus H. Selective enhancement of topologically induced interface states in a dielectric resonator chain. Nat Commun 2015;6:6710.
[47] Sinev IS, Mukhin IS, Slobozhanyuk AP, et al. Mapping plasmonic topological states at the nanoscale. Nanoscale 2015;7:11904–8.
[48] Kruk S, Slobozhanyuk A, Denkova D, et al. Edge states and topological phase transitions in chains of dielectric nanoparticles. Small 2017;13:1603190.
[49] Schomerus H. Topologically protected midgap states in complex photonic lattices. Opt Lett 2013;38:1912–4.
[50] Malzard S, Schomerus H. Nonlinear mode competition and symmetry-protected power oscillations in topological lasers. New J Phys 2018;20:063044.
[51] Poddubny A, Miroshnichenko A, Slobozhanyuk A, Kivshar Y. Topological majorana states in zigzag chains of plasmonic nanoparticles. ACS Photonics 2014;1:101–5.
[52] Pilozzi L, Conti C. Topological lasing in resonant photonic structures. Phys Rev B 2016;93:195317.
[53] Alpeggiani F, Andreani LC, Gerace D. Effective bichromatic potential for ultra-high Q-factor photonic crystal slab cavities. Appl Phys Lett 2015;107:261110.
[54] Simbula A, Schatzl M, Zagaglia L. Realization of high-Q/V photonic crystal cavities defined by an effective Aubry-André-Harper bichromatic potential. APL Photonics 2017;2:056102.
[55] Alpeggiani F, Kuipers L. Topological edge states in bichromatic photonic crystals. Optica 2019;6:96–103.
[56] Benalcazar WA, Bernevig BA, Hughes TL. Quantized electric multipole insulators. Science 2017;357:61–6.
[57] Benalcazar WA, Bernevig BA, Hughes TL. Electric multipole moments, topological multipole moment pumping, and chiral hinge states in crystalline insulators. Phys Rev B 2017;96:245115.
[58] Peterson CW, Benalcazar WA, Hughes TL, Bahl G. A quantized microwave quadrupole insulator with topologically protected corner states. Nature 2018;555:346–50.
[59] Xie B-Y, Wang H-F, Wang H-X, et al. Second-order photonic topological insulator with corner states. Phys Rev B 2018;98:205147.
[60] Noh J, Benalcazar WA, Huang S, et al. Topological protection of photonic mid-gap defect modes. Nat Photonics 2018;12:408–15.
[61] Xie B, Su G, Wang H, Su H, Shen X, Zhan P. Visualization of higher-order topological insulating phases in two-dimensional dielectric photonic crystals. Phys Rev Lett 2019;122:233903.
[62] El Hassan A, Kunst FK, Moritz A, Andler G, Bergholtz EJ, Bourennane M. Corner states of light in photonic waveguides. Nat Photonics 2019;13:697–700.
[63] Mittal S, Orre VV, Zhu G, Gorlach MA, Poddubny A, Hafezi M. Photonic quadrupole topological phases. Nat Photonics 2019;13:692–6.
[64] Chen XD, Deng WM, Shi FL, Zhao FL, Chen M, Dong JW. Direct observation of corner states in second-order topological photonic crystal slabs. Phys Rev Lett 2019;122:233902.
[65] Ota Y, Liu F, Katsumi R, et al. Photonic crystal nanocavity based on a topological corner state. Optica 2019;6:786–9.
[66] Ji C-Y, Liu G-B, Zhang Y, Zou B, Yao Y. Transport tuning of photonic topological edge states by optical cavities. Phys Rev A 2019;99:043801.
[67] Li F-F, Wang H-X, Xiong Z, et al. Topological light-trapping on a dislocation. Nat Commun 2018;9:2462.
[68] Xiao M, Zhang ZQ, Chan CT. Surface impedance and bulk band geometric phases in one-dimensional systems. Phys Rev X 2014;4:021017.
[69] Kalozoumis PA, Theocharis G, Achilleos V, Félix S, Richoux O, Pagneux V. Finite-size effects on topological interface states in one-dimensional scattering systems. Phys Rev A 2018;98:023838.
[70] Liu F, Deng H, Wakabayashi K. Topological photonic crystals with zero Berry curvature. Phys Rev B 2018;97:035442.
[71] Gorlach AA, Zhirihin DV, Slobozhanyuk AP, Khanikaev AB, Gorlach MA. Photonic Jackiw-Rebbi states in all-dielectric structures controlled by bianisotropy. Phys Rev B 2019;99:205122.
[72] Wang Z, Chong YD, Joannopoulos JD, Soljačić M. Reflection-free one-way edge modes in a gyromagnetic photonic crystal. Phys Rev Lett 2008;100:013905.
[73] Harari G, Bandres MA, Lumer Y, et al. Topological insulator laser: theory. Science 2018;359:eaar4003.
[74] Kavokin A, Malpuech G, Glazov M. Optical spin hall effect. Phys Rev Lett 2005;95:136601.
[75] Sala VG, Solnyshkov DD, Carusotto I, et al. Spin-Orbit coupling for photons and polaritons in microstructures. Phys Rev X 2015;5:011034.
[76] Nalitov AV, Solnyshkov DD, Malpuech G. Polariton Z topological insulator. Phys Rev Lett 2015;114:116401.

[77] Kartashov YV, Skryabin DV. Two-dimensional topological polariton laser. Phys Rev Lett 2019;122:083902.
[78] Karzig T, Bardyn C-E, Lindner NH, Refael G. Topological polaritons. Phys Rev X 2015;5:031001.
[79] Schneider C, Rahimi-Iman A, Kim NY, et al. An electrically pumped polariton laser. Nature 2013;497:348–52.
[80] Carusotto I, Ciuti C. Quantum fluids of light. Rev Mod Phys 2013;85:299–366.
[81] Kartashov YV, Skryabin DV. Modulational instability and solitary waves in polariton topological insulators. Optica 2016;3:1228–36.
[82] Kartashov YV, Skryabin DV. Bistable topological insulator with exciton-polaritons. Phys Rev Lett 2017;119:253904.
[83] Kane CL, Mele EJ. Z2 topological order and the quantum spin hall effect. Phys Rev Lett 2005;95:146802.
[84] Kane CL, Mele EJ. Quantum spin hall effect in graphene. Phys Rev Lett 2005;95:226801.
[85] Bernevig BA, Hughes TL, Zhang S-C. Quantum spin hall effect and topological phase transition in HgTe quantum wells. Science 2006;314:1757–61.
[86] Schnyder AP, Ryu S, Furusaki A, Ludwig AWW. Classification of topological insulators and superconductors in three spatial dimensions. Phys Rev B 2008;78:195125.
[87] Kitaev A, Lebedev V, Feigel'man M. Periodic table for topological insulators and superconductors. In AIP Conference Proceedings (AIP, 2009), pp. 22–30.
[88] Seclì M, Capone M, Carusotto I. Theory of chiral edge state lasing in a two-dimensional topological system. 2019. arXiv: 1901.01290. https://arxiv.org/abs/1901.01290.
[89] Seclì M. Edge state lasing in a 2D topological photonic system. Master thesis. Trento, Italy, University of Trento, 2017.
[90] Moiseyev N. Non-Hermitian quantum mechanics. Cambridge, UK, Cambridge University Press, 2011. https://doi.org/10.1017/CBO9780511976186.
[91] Bender CM, Boettcher S. Real spectra in non-hermitian hamiltonians having PT symmetry. Phys Rev Lett 1998;80:5243–6.
[92] Makris KG, El-Ganainy R, Christodoulides DN, Musslimani ZH. Beam dynamics in PT symmetric optical lattices. Phys Rev Lett 2008;100:103904.
[93] Feng L, El-Ganainy R, Ge L. Non-Hermitian photonics based on parity–time symmetry. Nat Photonics 2017;11:752–62.
[94] El-Ganainy R, Makris KG, Khajavikhan M, Musslimani ZH, Rotter S, Christodoulides DN. Non-Hermitian physics and PT symmetry. Nat Phys 2018;14:11–9.
[95] Özdemir K, Rotter S, Nori F, Yang L. Parity–time symmetry and exceptional points in photonics. Nat Mater 2019;18:783–98.
[96] Su WP, Schrieffer JR, Heeger AJ. Solitons in polyacetylene. Phys Rev Lett 1979;42:1698–701.
[97] Klett M, Cartarius H, Dast D, Main J, Wunner G. Relation between PT -symmetry breaking and topologically nontrivial phases in the Su-Schrieffer-Heeger and Kitaev models. Phys Rev A 2017;95:053626.
[98] Yuce C. Edge states at the interface of non-Hermitian systems. Phys Rev A 2018;97:042118.
[99] Zak J. Berrys phase for energy bands in solids. Phys Rev Lett 1989;62:2747–50.
[100] Rudner MS, Levitov LS. Topological transition in a non-hermitian quantum walk. Phys Rev Lett 2009;102:065703.
[101] Yin C, Jiang H, Li L, Lü R, Chen S. Geometrical meaning of winding number and its characterization of topological phases in one-dimensional chiral non-Hermitian systems. Phys Rev A 2018;97:052115.
[102] Weimann S, Kremer M, Plotnik Y, et al. Topologically protected bound states in photonic parity–time-symmetric crystals. Nat Mater 2017;16:433–8.
[103] Song W, Sun W, Chen C, et al. Breakup and recovery of topological zero modes in finite non-Hermitian optical lattices. Phys Rev Lett 2019;123:165701.
[104] Takata K, Notomi M. Photonic topological insulating phase induced solely by gain and loss. Phys Rev Lett 2018;121:213902.
[105] Guo A, Salamo GJ, Duchesne D, et al. Observation of PT-symmetry breaking in complex optical potentials. Phys Rev Lett 2009;103:93902.
[106] Liang SD, Huang GY. Topological invariance and global Berry phase in non-Hermitian systems. Phys Rev A: At Mol Opt Phys 2013;87:012118.
[107] Esaki K, Sato M, Hasebe K, Kohmoto M. Edge states and topological phases in non-Hermitian systems. Phys Rev B: Condens Matter Mater Phys 2011;84:205128.
[108] Sato M, Hasebe K, Esaki K, Kohmoto M. Time-reversal symmetry in non-Hermitian systems. Prog Theor Phys 2012;127:937–74.
[109] Feng L, Wong ZJ, Ma R-M, Wang Y, Zhang X. Single-mode laser by parity-time symmetry breaking. Science 2014;80:972–5.
[110] Takata K, Notomi M. PT-Symmetric coupled-resonator waveguide based on buried heterostructure nanocavities. Phys Rev Appl 2017;7:054023.
[111] Zhou L, Wang QH, Wang H, Gong J. Dynamical quantum phase transitions in non-Hermitian lattices. Phys Rev A 2018;98:022129.
[112] Malzard S, Cancellieri E, Schomerus H. Topological dynamics and excitations in lasers and condensates with saturable gain or loss. Opt Express 2018;26:22506.
[113] Luo X-W, Zhang C. Higher-order topological corner states induced by gain and loss. Phys Rev Lett 2019;123:073601.
[114] Leykam D, Bliokh KY, Huang C, Chong YD, Nori F. Edge modes, degeneracies, and topological numbers in non-Hermitian systems. Phys Rev Lett 2017;118:28–30.
[115] Shen H, Zhen B, Fu L. Topological band theory for non-Hermitian Hamiltonians. Phys Rev Lett 2018;120:146402.
[116] Malzard S, Schomerus H. Bulk and edge-state arcs in non-Hermitian coupled-resonator arrays. Phys Rev A 2018;98:033807.
[117] Kawabata K, Shiozaki K, Ueda M. Anomalous helical edge states in a non-Hermitian Chern insulator. Phys Rev B 2018;98:165148.
[118] Kawabata K, Higashikawa S, Gong Z, Ashida Y, Ueda M. Topological unification of time-reversal and particle-hole symmetries in non-Hermitian physics. Nat Commun 2019;10:297.
[119] Carlström J, Bergholtz EJ. Exceptional links and twisted Fermi ribbons in non-Hermitian systems. Phys Rev A 2018;98:042114.
[120] Zhou H, Lee JY, Liu S, Zhen B. Exceptional surfaces in PT-symmetric non-Hermitian photonic systems. Optica 2019;6:190.
[121] Wang H, Ruan J, Zhang H. Non-Hermitian nodal-line semimetals with an anomalous bulk-boundary correspondence. Phys Rev B 2019;99:075130.
[122] Yang Z, Hu J. Non-Hermitian Hopf-link exceptional line semimetals. Phys Rev B 2019;99:081102.
[123] Arkinstall J, Teimourpour MH, Feng L, El-Ganainy R, Schomerus H. Topological tight-binding models from nontrivial square roots. Phys Rev B 2017;95:165109.

[124] Lieu S. Topological symmetry classes for non-Hermitian models and connections to the bosonic Bogoliubov-de Gennes equation. Phys Rev B 2018;98:115135.
[125] Kawabata K, Shiozaki K, Ueda M, Sato M. Symmetry and topology in non-Hermitian physics. Phys Rev X 2019;9:041015.
[126] Zhou H, Lee JY. Periodic table for topological bands with non-Hermitian symmetries. Phys Rev B 2019;99:235112.
[127] Altland A, Zirnbauer MR. Nonstandard symmetry classes in mesoscopic normal-superconducting hybrid structures. Phys Rev B 1997;55:1142–61.
[128] Ryu S, Schnyder AP, Furusaki A, Ludwig AWW. Topological insulators and superconductors: tenfold way and dimensional hierarchy. New J Phys 2010;12:065010.
[129] Hasan MZ, Kane CL. Colloquium: topological insulators. Rev Mod Phys 2010;82:3045–67.
[130] Qi X-L, Zhang S-C. Topological insulators and superconductors. Rev Mod Phys 2011;83:1057–110.
[131] Gong Z, Ashida Y, Kawabata K, Takasan K, Higashikawa S, Ueda M. Topological phases of non-Hermitian systems. Phys Rev X 2018;8:031079.
[132] Longhi S, Gatti D, Della Valle G. Robust light transport in non-Hermitian photonic lattices. Sci Rep 2015;5:13376.
[133] Longhi S, Gatti D, Della Valle G. Non-Hermitian transparency and one-way transport in low-dimensional lattices by an imaginary gauge field. Phys Rev B 2015;92:094204.
[134] Lee TE. Anomalous edge state in a non-Hermitian lattice. Phys Rev Lett 2016;116:133903.
[135] Herviou L, Bardarson JH, Regnault N. Defining a bulk-edge correspondence for non-Hermitian Hamiltonians via singular-value decomposition. Phys Rev A 2019;99:052118.
[136] Ghatak A, Das T. New topological invariants in non-Hermitian systems. J Phys Condens Matter 2019;31:263001.
[137] Yokomizo K, Murakami S. Non-Bloch band theory of non-Hermitian systems. Phys Rev Lett 2019;123:066404.
[138] Yao S, Song F, Wang Z. Non-Hermitian Chern bands. Phys Rev Lett 2018;121:136802.
[139] Yao S, Wang Z. Edge states and topological invariants of non-Hermitian systems. Phys Rev Lett 2018;121:086803.
[140] Kunst FK, Edvardsson E, Budich JC, Bergholtz EJ. Biorthogonal bulk-boundary correspondence in non-Hermitian systems. Phys Rev Lett 2018;121:026808.
[141] Martinez Alvarez VM, Barrios Vargas JE, Foa Torres LEF. Non-Hermitian robust edge states in one dimension: anomalous localization and eigenspace condensation at exceptional points. Phys Rev B 2018;97:121401.
[142] Jin L, Song Z. Bulk-boundary correspondence in a non-Hermitian system in one dimension with chiral inversion symmetry. Phys Rev B 2019;99:081103.
[143] Wang P, Jin L, Song Z. Non-Hermitian phase transition and eigenstate localization induced by asymmetric coupling. Phys Rev A 2019;99:062112.
[144] Ozcakmakli Turker Z, Yuce C. Open and closed boundaries in non-Hermitian topological systems. Phys Rev A 2019;99:022127.
[145] Lee CH, Thomale R. Anatomy of skin modes and topology in non-Hermitian systems. Phys Rev B 2019;99:201103.
[146] Hatano N, Nelson DR. Localization transitions in non-hermitian quantum mechanics. Phys Rev Lett 1996;77:570–3.
[147] Ge Z-Y, Zhang Y-R, Liu T, Li S-W, Fan H, Nori F. Topological band theory for non-Hermitian systems from the Dirac equation. Phys Rev B 2019;100:054105.
[148] Okuma N, Kawabata K, Shiozaki K, Sato M. Topological origin of non-Hermitian skin effects. 2019. arXiv: 1910.02878. https://arxiv.org/abs/1910.02878.
[149] Heiss WD. Repulsion of resonance states and exceptional points. Phys Rev E Stat Phys Plasmas Fluids Relat Interdiscip Top 2000;61:929–32.
[150] Heiss WD. The physics of exceptional points. J Phys A Math Theor 2012;45:444016.
[151] Dembowski C, Gräf HD, Harney HL, et al. Experimental observation of the topological structure of exceptional points. Phys Rev Lett 2001;86:787–90.
[152] Zhen B, Hsu CW, Igarashi Y, et al. Spawning rings of exceptional points out of Dirac cones. Nature 2015;525:354–8.
[153] Hodaei H, Hassan AU, Wittek S. Enhanced sensitivity at higher-order exceptional points. Nature 2017;548:187–91.
[154] Chen W, Kaya Özdemir Ş, Zhao G, Wiersig J, Yang L. Exceptional points enhance sensing in an optical microcavity. Nature 2017;548:192–6.
[155] Assawaworrarit S, Yu X, Fan S. Robust wireless power transfer using a nonlinear parity-time-symmetric circuit. Nature 2017;546:387–90.
[156] Kawabata K, Bessho T, Sato M. Classification of exceptional points and non-Hermitian topological semimetals. Phys Rev Lett 2019;123:066405.
[157] Lin S, Jin L, Song Z. Symmetry protected topological phases characterized by isolated exceptional points. Phys Rev B 2019;99:165148.
[158] Yuce C. Topological states at exceptional points. Phys Lett Sect A Gen At Solid State Phys 2019;383:2567–70.
[159] Yoshida T, Hatsugai Y. Exceptional rings protected by emergent symmetry for mechanical systems. Phys Rev B 2019;100:054109.
[160] Malzard S, Poli C, Schomerus H. Topologically protected defect states in open photonic systems with non-Hermitian charge-conjugation and parity-time symmetry. Phys Rev Lett 2015;115:200402.
[161] Zhao H, Longhi S, Feng L. Robust light state by quantum phase transition in non-Hermitian optical materials. Sci Rep 2015;5:17022.
[162] Pan M, Zhao H, Miao P, Longhi S, Feng L. Photonic zero mode in a non-Hermitian photonic lattice. Nat Commun 2018;9:1308.
[163] Zhou H, Peng C, Yoon Y, et al. Observation of bulk Fermi arc and polarization half charge from paired exceptional points. Science 2018;359:1009–12.
[164] Zhao H, Qiao X, Wu T, Midya B, Longhi S, Feng L. Non-Hermitian topological light steering. Science 2019;365:1163–6.